

AD-A201 292

FILE COPY

2

AFWAL-TR-88-2095

## In-Line Wear Monitor



Keith Pleper  
Allison Gas Turbine Division  
P.O. Box 420  
Indianapolis, IN 46260-0420

Dr. Ivor J. Taylor  
Princeton Gamma-Tech  
1200 State Rd  
Princeton, NJ 08540

November 1988

Interim Technical Report  
for Period November 1985-June 1988

Approved for public release; distribution unlimited.



88 12 13 1988

Aero Propulsion Laboratory  
Air Force Wright Aeronautical Laboratories  
Air Force Systems Command  
Wright-Patterson Air Force Base, OH 45433-6563

UNCLASSIFIED

SECURITY CLASSIFICATION OF THIS PAGE

## REPORT DOCUMENTATION PAGE

1a. REPORT SECURITY CLASSIFICATION UNCLASSIFIED			1b. RESTRICTIVE MARKINGS None		
2a. SECURITY CLASSIFICATION AUTHORITY			3. DISTRIBUTION/AVAILABILITY OF REPORT Approved for public release; distribution unlimited		
2b. DECLASSIFICATION/DOWNGRADING SCHEDULE					
4. PERFORMING ORGANIZATION REPORT NUMBER(S) EDR 13632			5. MONITORING ORGANIZATION REPORT NUMBER(S) AFWAL-TR-88-2095		
6a. NAME OF PERFORMING ORGANIZATION Allison Gas Turbine Division		6b. OFFICE SYMBOL (If applicable)	7a. NAME OF MONITORING ORGANIZATION Aero Propulsion Laboratory (AFWAL/POSL) Air Force Wright Aeronautical Laboratories		
6c. ADDRESS (City, State and ZIP Code) P.O. Box 420 Indianapolis, IN 46206-0420			7b. ADDRESS (City, State and ZIP Code) Wright-Patterson AFB, OH 45433-6563		
8a. NAME OF FUNDING/SPONSORING ORGANIZATION		8b. OFFICE SYMBOL (If applicable)	9. PROCUREMENT INSTRUMENT IDENTIFICATION NUMBER Contract No. F33615-85-C-2537		
8c. ADDRESS (City, State and ZIP Code)			10. SOURCE OF FUNDING NOS		
			PROGRAM ELEMENT NO	PROJECT NO	TASK NO
11. TITLE (Include Security Classification) In-Line Wear Monitor			62203F	3048	06
12. PERSONAL AUTHOR(S) Keith A. Pieper and Dr. Ivor J. Taylor					
13a. TYPE OF REPORT Interim Technical		13b. TIME COVERED FROM 11/85 TO 6/88		14. DATE OF REPORT (Yr., Mo., Day) November 1988	
15. PAGE COUNT 68					
16. SUPPLEMENTARY NOTATION					
17. COSATI CODES			18. SUBJECT TERMS (Continue on reverse if necessary and identify by block number)		
FIELD	GROUP	SUB GR.	Debris, diagnostics, turbine, wear, lubrication, JE 5		
21	05				
14	04				
19. ABSTRACT (Continue on reverse if necessary and identify by block number) This report describes the construction and test results of an in-line monitor for critical ferrous and nonferrous metal debris in turbine engine lubrication systems. The in-line wear monitor (ILWM) is being developed by Allison Gas Turbine Division and a subcontractor, Princeton Gamma-Tech. The system uses the X-ray fluorescence principle for detecting metal debris on a continuous basis while the engine is running. The sensor portion of the system is engine mounted and contains a radioactive X-ray source, a flow cell to direct the oil across an X-ray permeable window, a proportional counter X-ray detector and its associated preamplifier and amplifier electronics. The data acquisition electronics is mounted on the airframe and contains a microprocessor based system for inputting pulses from the sensor, classifying and counting them according to energy bands, and analyzing the data and outputting metal concentration values to the engine monitoring system.					
(cont)					
20. DISTRIBUTION/AVAILABILITY OF ABSTRACT UNCLASSIFIED/UNLIMITED <input checked="" type="checkbox"/> SAME AS RPT. <input type="checkbox"/> DTIC USERS <input type="checkbox"/>			21. ABSTRACT SECURITY CLASSIFICATION UNCLASSIFIED		
22a. NAME OF RESPONSIBLE INDIVIDUAL Dr. Phillip W. Centers		22b. TELEPHONE NUMBER (Include Area Code) (513) 255-6608		22c. OFFICE SYMBOL AFWAL/POSL	

DD FORM 1473, 83 APR

EDITION OF 1 JAN 73 IS OBSOLETE.

†

UNCLASSIFIED  
SECURITY CLASSIFICATION OF THIS PAGE

**UNCLASSIFIED**

**SECURITY CLASSIFICATION OF THIS PAGE**

The sensor portion of the system is designed to fit on a TF41 turbine engine in place of a tube between the oil tank and the oil pump. The critical preamplifier and high voltage power supply circuits have been demonstrated to be stable at high temperature ambients.

The sensor has been developed to have a very low iron background count and application testing has been demonstrated to have high enough sensitivity to be capable of detecting iron down to the 2-5 ppm level with static oil samples.

The sensor has been vibration tested with sinusoidal sweeps and with random vibration profiles typical on a TF41 engine. The sensor was not damaged by the vibration but was found to have resonances that affected the output signal.

The plans for the remainder of the program include changes to the preamplifier hardware to reduce resonance effects, flow testing of the system with various metal concentrations and oil temperatures, and evaluation of the system on a TF41 engine test.

**UNCLASSIFIED**

**SECURITY CLASSIFICATION OF THIS PAGE**

TABLE OF CONTENTS

<u>Section</u>	<u>Title</u>	<u>Page</u>
I	INTRODUCTION . . . . .	1
II	PROGRAM BACKGROUND . . . . .	2
III	SENSOR MECHANICAL DESIGN . . . . .	4
IV	SENSOR ELECTRONIC DESIGN . . . . .	10
	4.1 Preamplifier . . . . .	10
	4.2 High Voltage Power Supply . . . . .	10
	4.3 Amplifier Electronics . . . . .	10
	4.4 Analysis Electronics . . . . .	10
V	SENSOR APPLICATION TESTING . . . . .	16
	5.1 Initial Sensitivity Testing . . . . .	16
	5.2 Flow Cell Testing . . . . .	17
	5.3 Detectability Limits in Water and Oil . . . . .	21
	5.4 Beryllium Window Contamination . . . . .	27
VI	SENSOR VIBRATION TESTING . . . . .	33
	6.1 Sensor Mounting . . . . .	33
	6.2 Vibration Test Results . . . . .	33
VII	SENSOR FLOW EVALUATION . . . . .	59
VIII	CONCLUSIONS AND PLANS . . . . .	60
	REFERENCES . . . . .	61

Accession For	
NTIS GRA&I	<input checked="" type="checkbox"/>
DTIC TAB	<input type="checkbox"/>
Unannounced	<input type="checkbox"/>
Justification	
By _____	
Distribution/	
Availability Codes	
Dist	Avail and/or Special
A-1	



## LIST OF ILLUSTRATIONS

<u>Figure</u>	<u>Title</u>	<u>Page</u>
1	In-Line Wear Monitor Program schedule . . . . .	2
2	In-line wear monitor block diagram . . . . .	3
3	Oil tube location on TF41 engine . . . . .	5
4	Flow cell, electronics, and counter tube . . . . .	6
5	Assembled electronics housing . . . . .	6
6	Electronics housing . . . . .	7
7	Electronics assembled to base plate . . . . .	7
8	Radioactive source data sheet . . . . .	8
9	Preamplifier schematic . . . . .	11
10	Preamplifier temperature effects . . . . .	12
11	High voltage power supply schematic . . . . .	13
12	High voltage power supply temperature effects . . . . .	14
13	Data processing electronics block diagram . . . . .	15
14	Background spectrum from beryllium foil window . . . . .	18
15	Background spectrum from air . . . . .	19
16	Background spectrum from polyimide window . . . . .	19
17	Background spectra argon-xenon and neon-argon detectors . . . . .	20
18	Background spectrum 0 ppm sample, polyimide window . . . . .	21
19	Spectrum 200 ppm iron sample . . . . .	22
20	Spectra 100 ppm iron sample . . . . .	22
21	Expanded spectrum 100 ppm sample . . . . .	23
22	Spectra 10 ppm iron sample . . . . .	24
23	Spectra 20 ppm iron sample . . . . .	25
24	Data and response curve--polyimide window . . . . .	26
25	Backscatter spectra from beryllium foils . . . . .	28
26	Beryllium foil data sheet . . . . .	29
27	Spectra of clean beryllium compared to polyimide window . . . . .	31
28	Data and response curve--clean beryllium window . . . . .	32
29	Spectrum from the sensor--copper foil cell window . . . . .	34
30	Sensor mounting orientation for vibration tests . . . . .	34
31	Resonance profile--vertical vibration sweep . . . . .	35
32	Spectrum at 265 Hz resonance . . . . .	36
33	Spectrum at 732 Hz resonance . . . . .	37
34	Spectrum at 1235 Hz resonance . . . . .	38
35	Spectrum at 1637 Hz resonance . . . . .	39
36	Resonance profile--lateral vibration sweep . . . . .	39
37	Resonance profile--axial vibration sweep . . . . .	40
38	Spectrum at 625 Hz resonance . . . . .	40
39	Spectrum at 1187 Hz resonance . . . . .	41
40	Spectrum with test pulses into sensor--copper foil window removed . . . . .	42
41	Resonance profile--vertical vibration sweep--no cell window . . . . .	43
42	Spectrum at 712.5 Hz resonance . . . . .	43
43	Spectra at 701 Hz lateral resonance with and without detector HV bias . . . . .	44
44	Expanded display of Figure 43 . . . . .	45

LIST OF ILLUSTRATIONS (concluded)

<u>Figure</u>	<u>Title</u>	<u>Page</u>
45	Resonance profile--vertical vibration sweep, copper foil cell window replaced, circuit boards conformally coated .	45
46	Spectrum at the 680 Hz resonance . . . . .	47
47	Spectrum at the 712 Hz resonance . . . . .	48
48	Comparison of A1 208 (Figure 33) and A1 224 (Figure 47) . .	49
49	Spectrum at the 1237 Hz (5.9 g) resonance . . . . .	50
50	Comparison of A1 209 (Figure 34) and A1 225 (Figure 49) . .	51
51	NAVMAT vibration profile . . . . .	52
52	Resonance profile--vertical vibration NAVMAT . . . . .	52
53	Resonance profile--lateral vibration--NAVMAT . . . . .	53
54	Resonance profile--axial vibration--NAVMAT repeated test . . . . .	53
55	Spectrum taken during NAVMAT vibration . . . . .	55
56	Resonance profile--vertical vibration sweep sensor unit only--cell removed . . . . .	55
57	Spectrum at 2775 Hz (38 g) resonance . . . . .	56
58	Simulated TF41 engine vibration profile . . . . .	57
59	Pulse envelope . . . . .	58

## I. INTRODUCTION

The purpose of this interim technical report is to describe the current technology of the In-Line Wear Monitor program. The technology described was developed during the time period 15 November 1985 to 30 June 1988 as a part of Air Force contract F33615-85-C-2537.

The objective of this program is to design, construct, evaluate, and demonstrate an in-line monitor for critical ferrous and nonferrous debris in turbine engine lubrication systems under engine operating conditions.

The development of an effective monitoring system for wear debris would reduce the need for oil sampling followed by laboratory spectrometric analysis as now performed in the military Joint Oil Analysis program (JOAP). This program builds on previous contracts sponsored by the Air Force (Ref 1\* and 2) that demonstrated the detection of iron in oil using the X-ray fluorescence principle. This program goes beyond the previous programs by developing a sensor system that can be mounted on an engine and operate under the severe environment present on the engine. The aim of the program is to develop and engine demonstrate a device that with minor modification can be flight demonstrated in a follow-on program. Once the device is flight demonstrated it can then be specified with some confidence for new engine programs. Because of the desire to eventually flight demonstrate the device, the device was made compatible with an engine for which an engine monitoring system was already available.

The underlying technology selected to detect the metallic debris in oil was X-ray fluorescence. The oil is irradiated by an X-ray source, and the X-rays strike the wear metal atoms in the oil causing them to emit secondary X-rays with an energy indicative of the type of metal and a frequency of occurrence indicative of concentration.

Section II of this report briefly describes program background. Sections III and IV describe the mechanical and electronic design details of the system being developed. Sections V, VI, and VII describe the results of application, vibration, and flow testing of the sensor. Section VIII gives the conclusions reached at this point in the program and indicates the plans for further development.

---

\*References are listed at the end of this report.

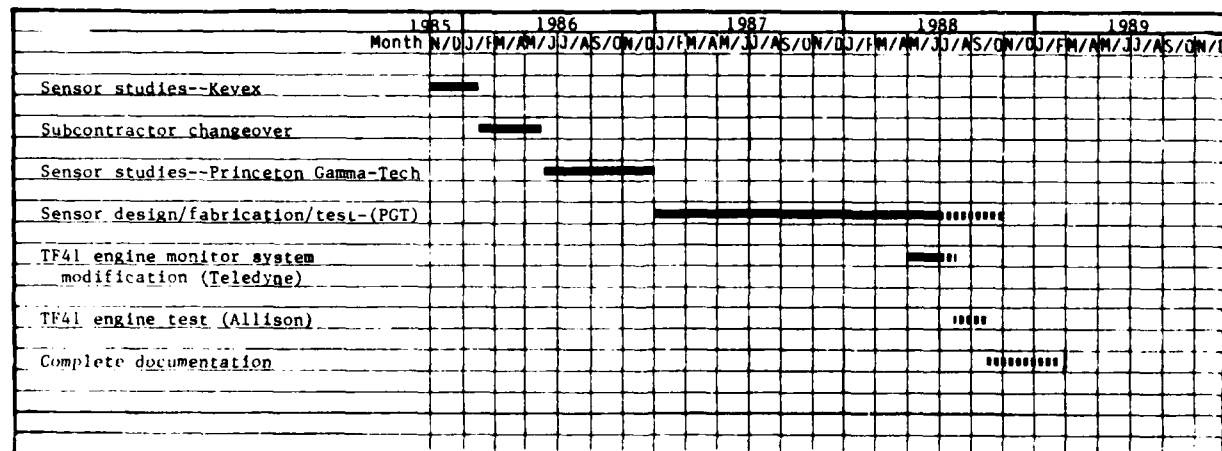
## II. PROGRAM BACKGROUND

In November 1985, Allison started work on contract F33615-85-C-2537 to design, construct, demonstrate, and deliver a working model of an in-line wear monitor (ILWM) for metallic debris in engine oil. The program activity to date is indicated in Figure 1. Initially Kevex Corporation was selected as a subcontractor to develop the X-ray fluorescent technology needed for the sensor. After review of several detector technologies, Kevex selected silicon X-ray detector technology coupled with thermionic cooling for development. Kevex acquired several detectors, thermoelectric cooling modules, X-ray sources, and test chamber equipment. Kevex performed preliminary testing to assess heat sink requirements.

Based on Kevex's findings concerning the difficulty in maintaining the silicon detector at near cryogenic temperatures without additional hardware for heat sinking--such as fuel cooling, it was decided that it was unlikely that a near flight demonstratable sensor could be developed in the time frame of this program. A second technology for X-ray detection, the use of proportional counter tubes, has been demonstrated on a previous Air Force program (Ref 1 and 2) with Pratt and Whitney. Proportional counter tubes with improved sensitivity made by the Finnish company Outokumpu had been used in the previous program, and it was felt the sensitivity was sufficient to detect trends in oil debris.

A second subcontractor, Princeton Gamma-Tech, which had been acquired by Outokumpu and therefore had access to the improved proportional counter technology, was contracted to develop the sensor starting in July 1986. Princeton Gamma-Tech arranged to have L. Packer of Pratt and Whitney and H. Sipila of Outokumpu serve as consultants since they had worked on the previous Air Force development programs and could contribute knowledge gained on the previous programs to the new monitor system.

A block diagram of the system being developed is shown in Figure 2. The sensor is to be engine mounted and contains a radioactive X-ray source, a flow cell to direct the oil across an X-ray permeable window, a proportional counter X-ray detector and its associated analog circuitry, a preamplifier, and



TE88-4813

Figure 1. In-Line Wear Monitor program schedule.

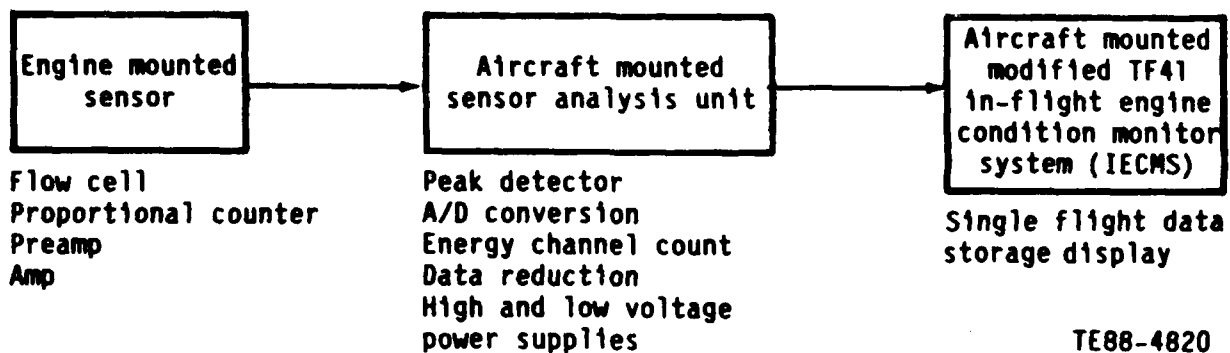


Figure 2. In-line wear monitor block diagram.

amplifier electronics. The data acquisition electronics is mounted off engine on the airframe and includes a peak detector, A/D converter, a microprocessor based section for keeping track of energy band counts and data analysis, high and low voltage power supplies, and system interface electronics. The data storage section consists of existing engine monitor system electronics that are to be modified to accept the outputs of the data acquisition electronics and store debris concentration values on magnetic tape for long term trending.

### III. SENSOR MECHANICAL DESIGN

The flow cell for the in-line wear monitor system was designed to fit in place of a tube going between the TF41 engine oil tank and the engine oil pump inlet. This location was selected because (1) it is easy to insert the flow cell at this point since the tube is easily removed, (2) the location sees the full oil flow of the system and is ahead of the oil filter, and (3) the oil pressure is low at this point--approximately 3 psi--which reduces the stress on the X-ray window. The tube being replaced is shown in the exploded view of the TF41 oil system in Figure 3 and the design of the flow cell is shown in Figures 4 and 5. The flow cell can be easily inserted in place of the original tube by removing four bolts that hold the mating connector assembly.

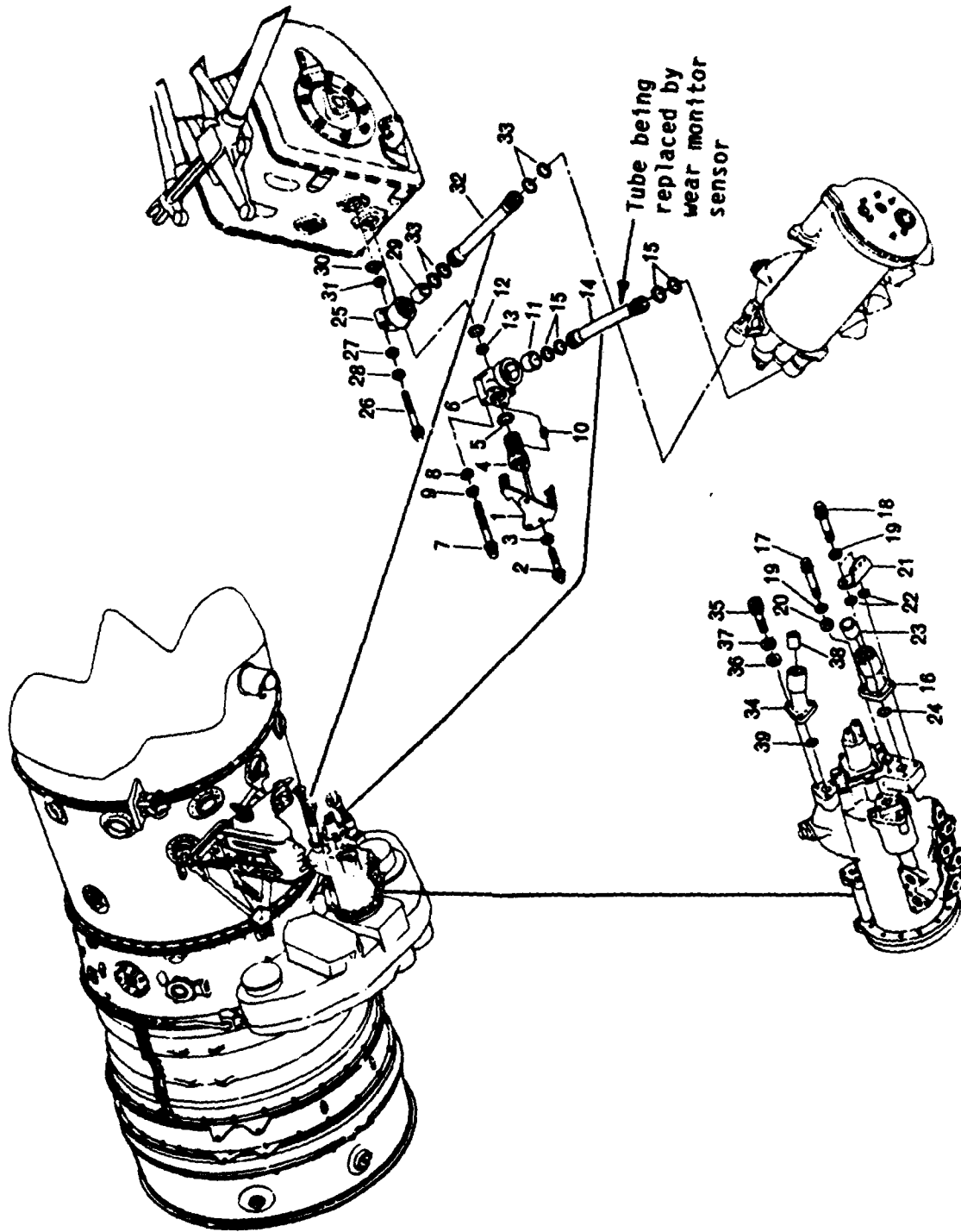
The TF41 engine uses MIL-L-23699 oil with a maximum steady state oil inlet temperature of 248°F (120°C), while the maximum transient oil inlet temperature is 311°F (155°C). Typical oil temperature after the fuel cooled oil cooler is 180°F (82°C). Oil flow rates on the TF41 typically go from 5.5 gal/minute at 60 percent  $N_H$  speed to 9.3 gal/minute at 100 percent  $N_H$ . Total oil in the engine system is 1.98 gal on the Air Force TF41-A-1 and 3.53 gal on the Navy TF41-A-2. Oil consumption rates can run 0.12 gal/hr. The small oil capacity and high consumption rate of the TF41 make debris concentration trending harder to do, although normal Spectrographic Oil Analysis program (SOAP) trending is still useful for indicating impending component failures.

The flow cell has been designed with end tube sections identical to the tube it replaces and a cylindrical section in the middle of the tube as shown in Figure 4. A circular X-ray permeable window is placed over the circular opening on top of the flow cell and sealed by an O-ring. An anvil-shaped oil flow deflector is attached to the bottom lid and serves to evenly direct part of the oil flow across the X-ray window. The oil flow deflector has holes drilled in it parallel to the direction of oil flow and sized so that the cross sectional area of the flow cell is the same as the original tube so as not to restrict oil flow. The flow cell was made of stainless steel as was the original tube and was machined out of a solid piece of stainless steel to maximize physical integrity. In this program a single radio isotope, proportional counter, and electronics capable of detecting iron and copper, is being developed. The way the flow cell is constructed, however, would allow a second radioisotope, proportional counter, and electronics capable of detecting additional metals, to be mounted on the bottom of the flow cell cylindrical section provided there is sufficient clearance on the engine for an additional electronics housing.

The housing that contains the proportional counter tube, the radio isotope sources, and the amplification electronics is shown in Figures 4 through 7. The housing attaches to the flow cell and is designed so that if the X-ray window between the housing and the flow cell breaks or leaks, the housing serves as a secondary containment so that engine oil will not be lost. The irregular shape of two of the corners of the housing was necessary so that the unit would clear other objects nearby on the TF41 engine.

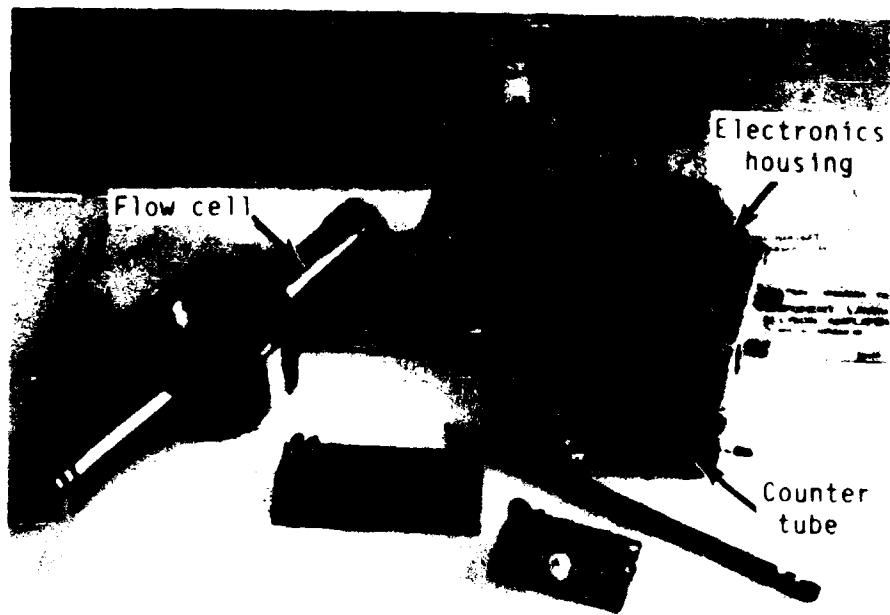
The special miniaturized proportional counter tubes developed for this project by Outokumpu and the electronic printed circuit boards, which mount in the sensor, are shown in Figures 4 through 7. The radioactive sources are curium-244 and are fabricated as two small disks of 30-millicurie strength. The radioactive sources are encapsulated as shown in Figure 8 so they cannot leak out of the sensor. The sources are mounted at an angle and shielded so

Oil system



TE88-4821

Figure 3. Oil tube location on TF41 engine.



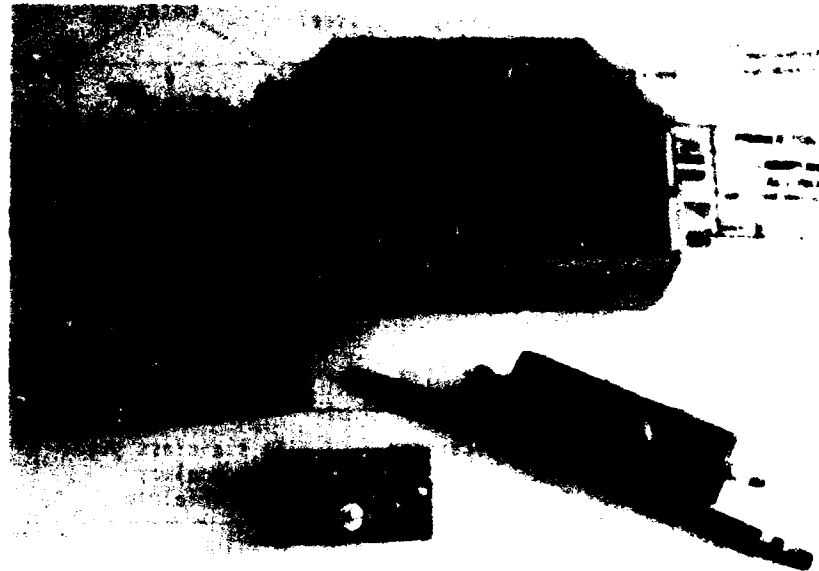
TE88-4822

Figure 4. Flow cell, electronics and counter tube.



TE88-4823

Figure 5. Assembled electronics housing.



TE88-4824

Figure 6. Electronics housing.



TE88-4825

Figure 7. Electronics assembled to base plate.

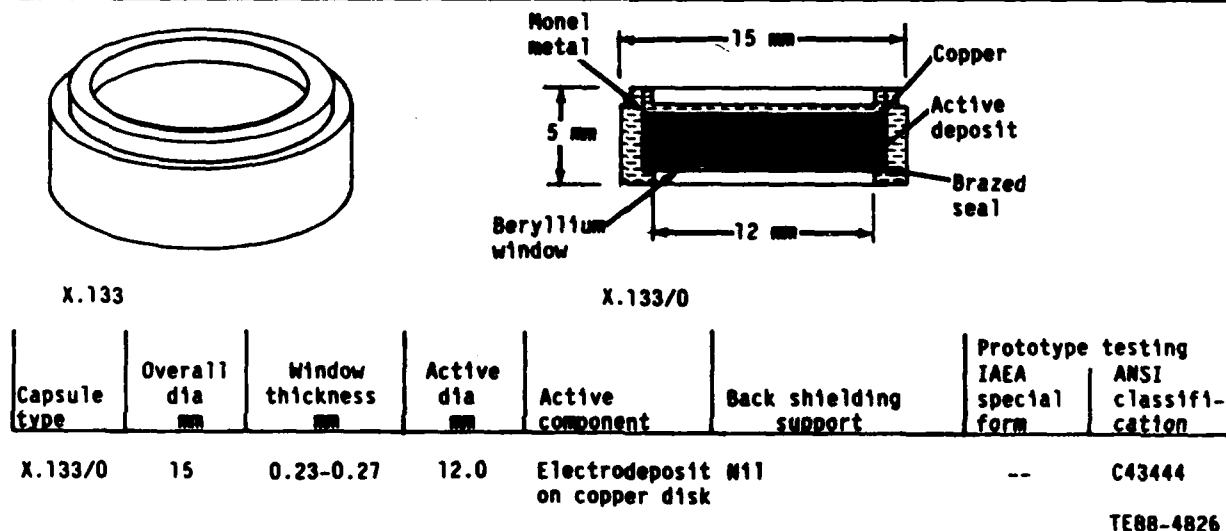
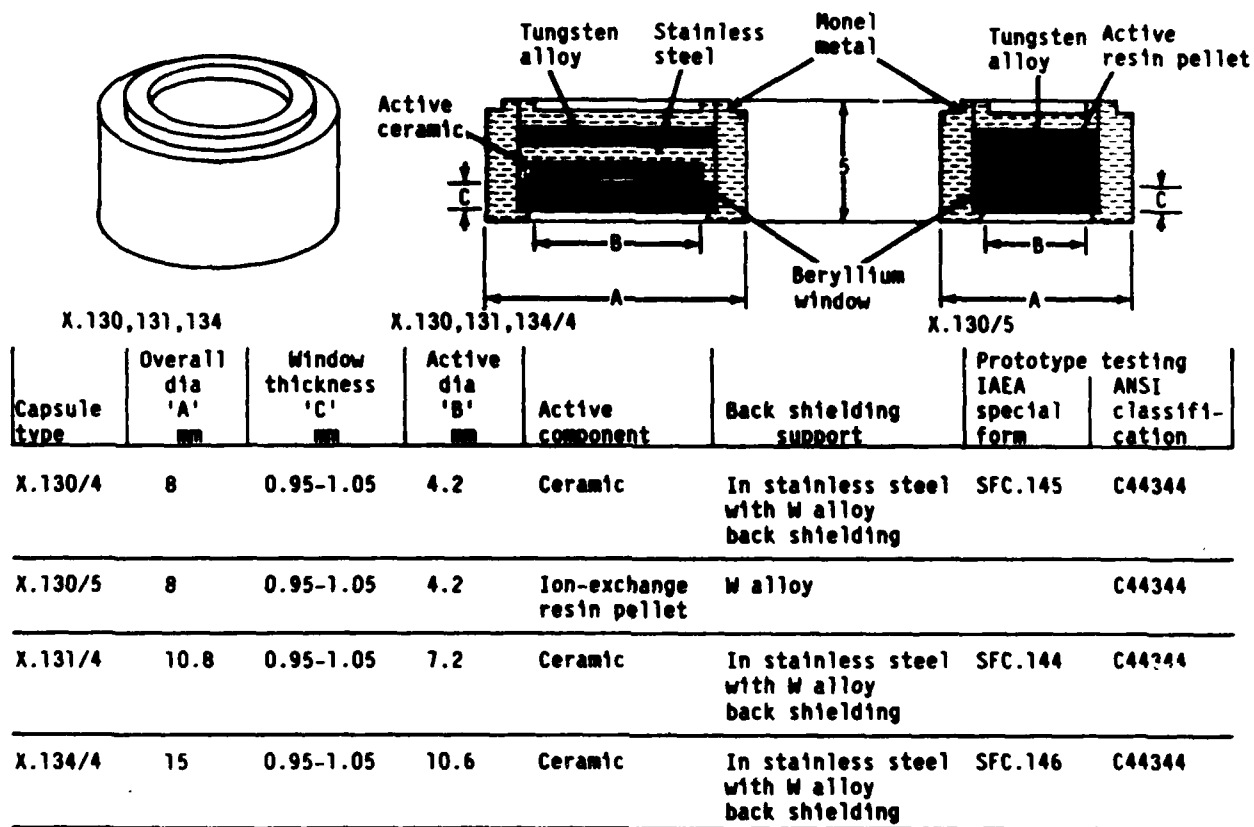


Figure 8. Radioactive source data sheet.

that a beam of X-rays strikes the oil at a shallow angle relative to the X-ray permeable window.

The proportional counter tubes contain a very thin anode wire usually made of tungsten and 13-25 micrometers in diameter. The tube is filled with a mixture of noble gas such as neon-argon or argon-xenon and is made of stainless steel lined with a second material such as high purity aluminum to prevent detection of impurities in the walls. The X-rays enter the tube through a high purity beryllium (Be) window that is brazed in place. A high voltage is connected between the anode and the case so that when X-rays strike the gas mixture ion pairs are created and collected as a series of short current pulses.

As discussed later in Section IV it was advantageous to keep the case of the counter tube at a high negative potential instead of biasing the anode at a high positive potential as is usually done. Thus the counter tube case had to be mounted on insulating blocks as shown in Figures 4, 6, and 7. To try to minimize microphonic effects (i.e., extraneous signal outputs due to vibration or acoustic noise), the preamplifier printed circuit board was designed to mount right on the end of the counter tube so that wire lengths could be minimized. The printed circuit boards are made with a teflon based material so that they can survive 150°C ambients without degradation. The boards are laid out using single-sided interconnections so that one side can be a ground plane to further minimize microphonics.

The entire sensor weighs 3.83 lb with the flow cell body contributing 1.63 lb and the electronics housing and boards 2.2 lb.

#### IV. SENSOR ELECTRONIC DESIGN

Much effort was expended by Princeton Gamma-Tech (PGT) in the September 1986 to July 1988 time period to develop preamplifier and high voltage power supply designs that would be stable up to 150°C, which is near the maximum transient oil inlet temperature on the TF41. It was later decided due to space limitations to locate the high voltage power supply with the off-engine mounted data acquisition electronics instead of in the sensor; however, the high stability design will still help reduce drift and is available for future use in designs with the power supply in the sensor if needed.

##### 4.1 PREAMPLIFIER

Two different preamplifier designs were high temperature tested. The lowest drift results were obtained with a previous PGT design modified to work with the proportional counter case at high negative voltage instead of keeping the counter's anode at a high positive voltage as was previously done. The configuration of preamplifier circuit that was temperature tested is shown in Figure 9. The circuit was temperature tested with several values of feedback resistance, as shown in Figure 10, to determine how large a value could be used without causing the output to saturate due to field effect transistor (FET) leakage currents. A 100 megaohm value allows operation through 175°C without saturation. In the final circuit a low noise 100 megaohm metal film feedback resistor was used.

##### 4.2 HIGH VOLTAGE POWER SUPPLY

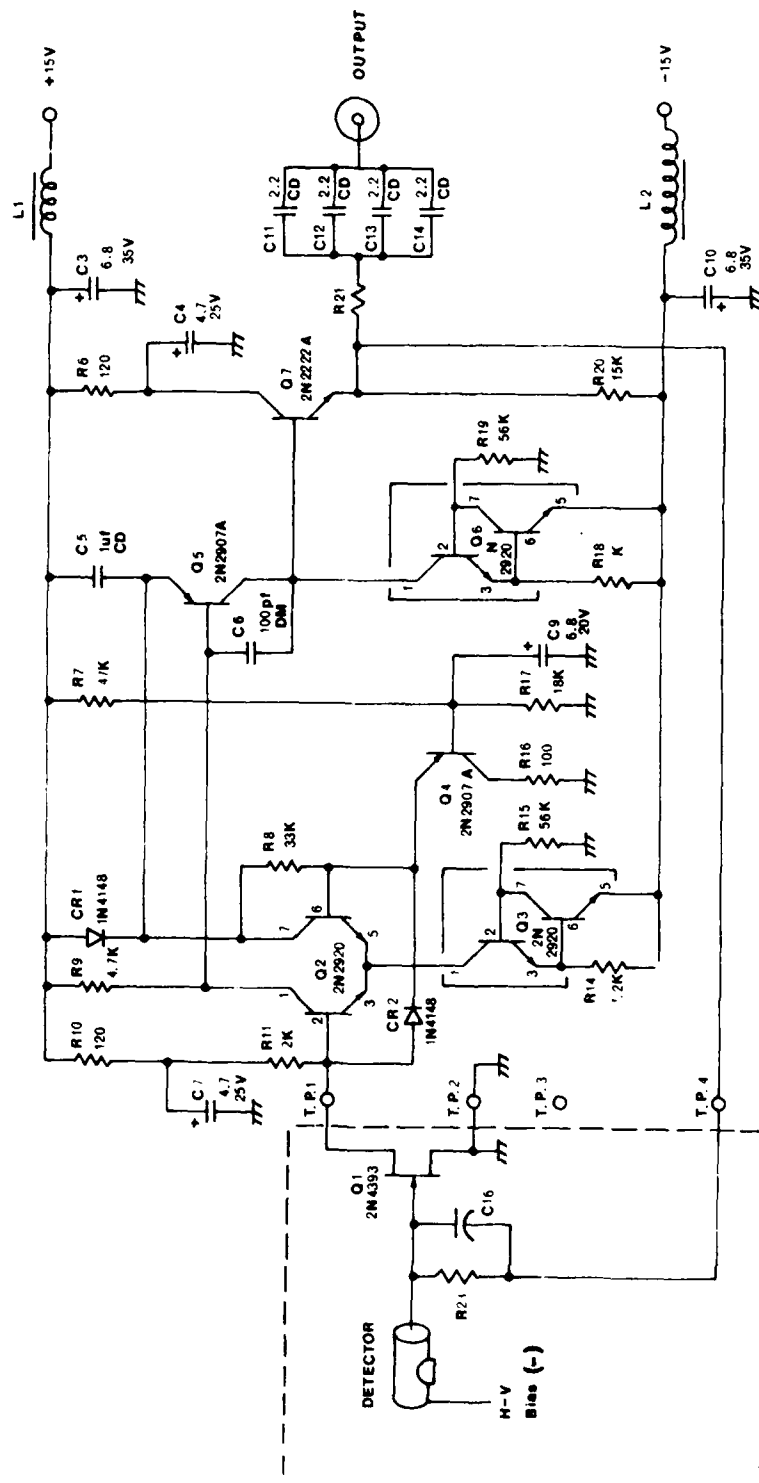
Several high voltage power supplies were evaluated for temperature stability with a design obtained from Outokumpu giving the least drift. The configuration of the supply circuit tested is shown in Figure 11. The test results, plotted in Figure 12, show essentially no drift up to about 120°C, which is adequate for the off-engine mounted sensor analysis unit. The stability of the high voltage supply is essential to prevent shifts in the gas gain of the proportional counter circuit as shown later in subsection 6.2.1.3, in which a shift of 2 V in the high voltage (HV) supply shifts the X-ray copper peak 0.5 kV or about 6 percent.

##### 4.3 AMPLIFIER ELECTRONICS

In addition to the preamplifier, the sensor head contains a signal processing amplifier with fast channel for pile-up and live time correction. The amplifier stage was included in the sensor head to increase the signal amplitude level from millivolts to volts so the signal can be transmitted through engine and aircraft wiring to the aircraft mounted analysis electronics with less chance of noise pickup.

##### 4.4 ANALYSIS ELECTRONICS

A diagram of the electronics being developed to process the pulse signals from the engine mounted sensor is shown in Figure 13. A peak detector circuit is used to capture the peak value of the pulse from the sensor head amplifier. The peak value is digitized by a special A/D converter designed to avoid non-linear effects of normal successive approximation converters. The digitized pulse value is used to increment the pulse counts of the corresponding energy band counter. After accumulating counts for a period of time, the results can

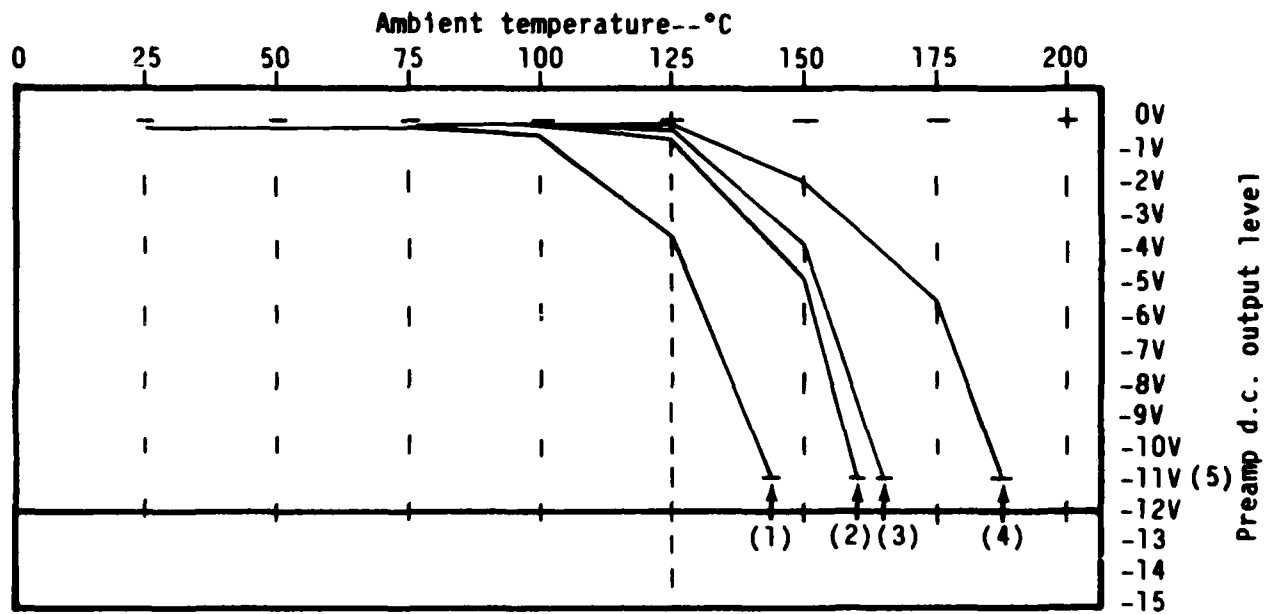


Notes: (Unless otherwise specified)

1. All resistors in ohms, RMC, 1/4W, 1%
2. All capacitors in uf's
3. Q2, Q7 are flight approved transistors
4. All electrolytics replaced with similar value ceramic capacitors

TE88-4827

Figure 9. Preamplifier schematic.



Notes for curves:

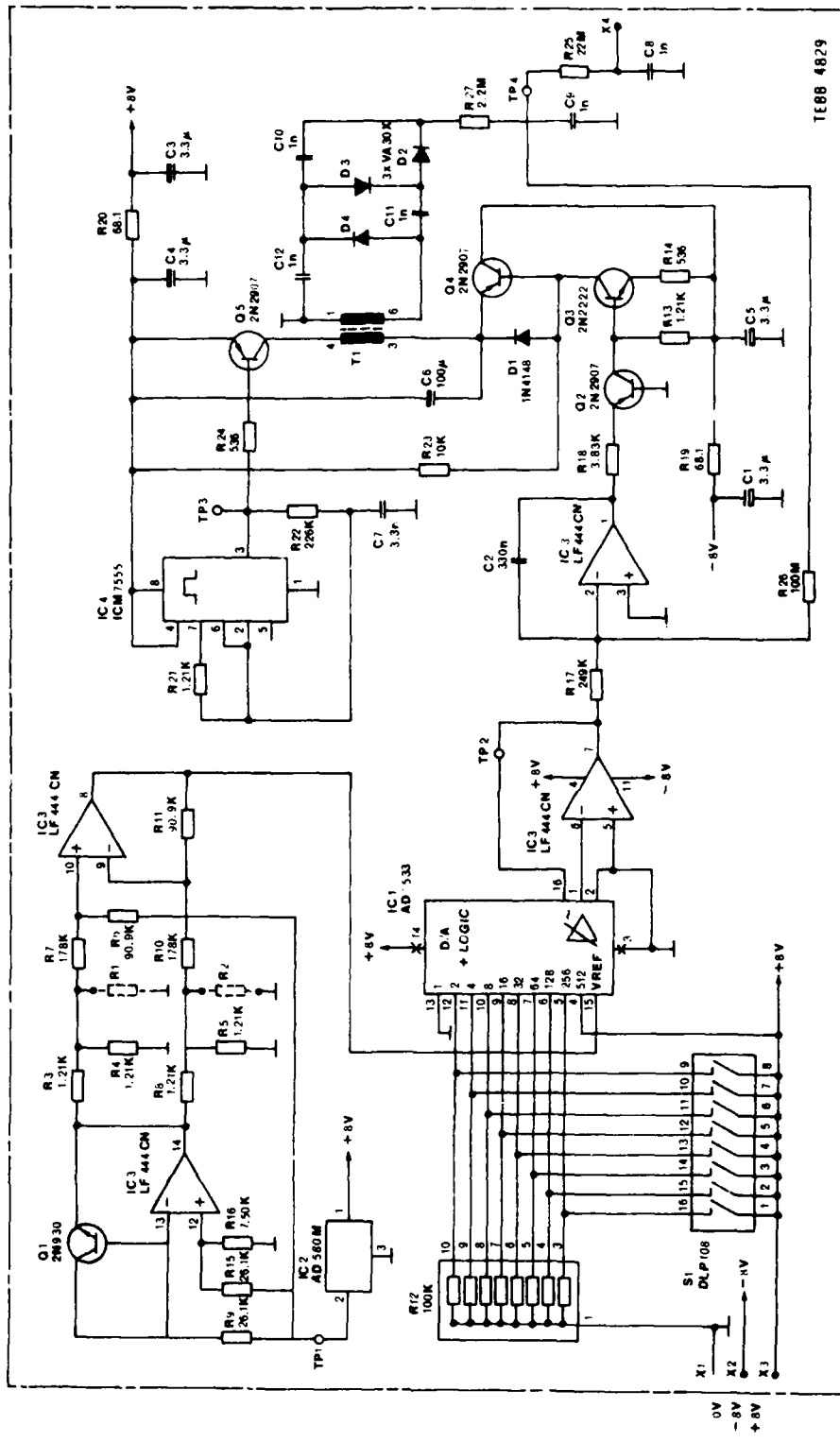
1. 2 giga ohm feedback resistor--glass construction
2. 500 mega ohm carbon composition
3. 2 giga ohm feedback with leakage balancing scheme
4. 100 mega ohm carbon composition
5. -11 volts is the limit for output d.c. voltage with a  $\pm 12$  volt power supply

Temperature effects on preamp behavior with various feedback networks

TE88-4828

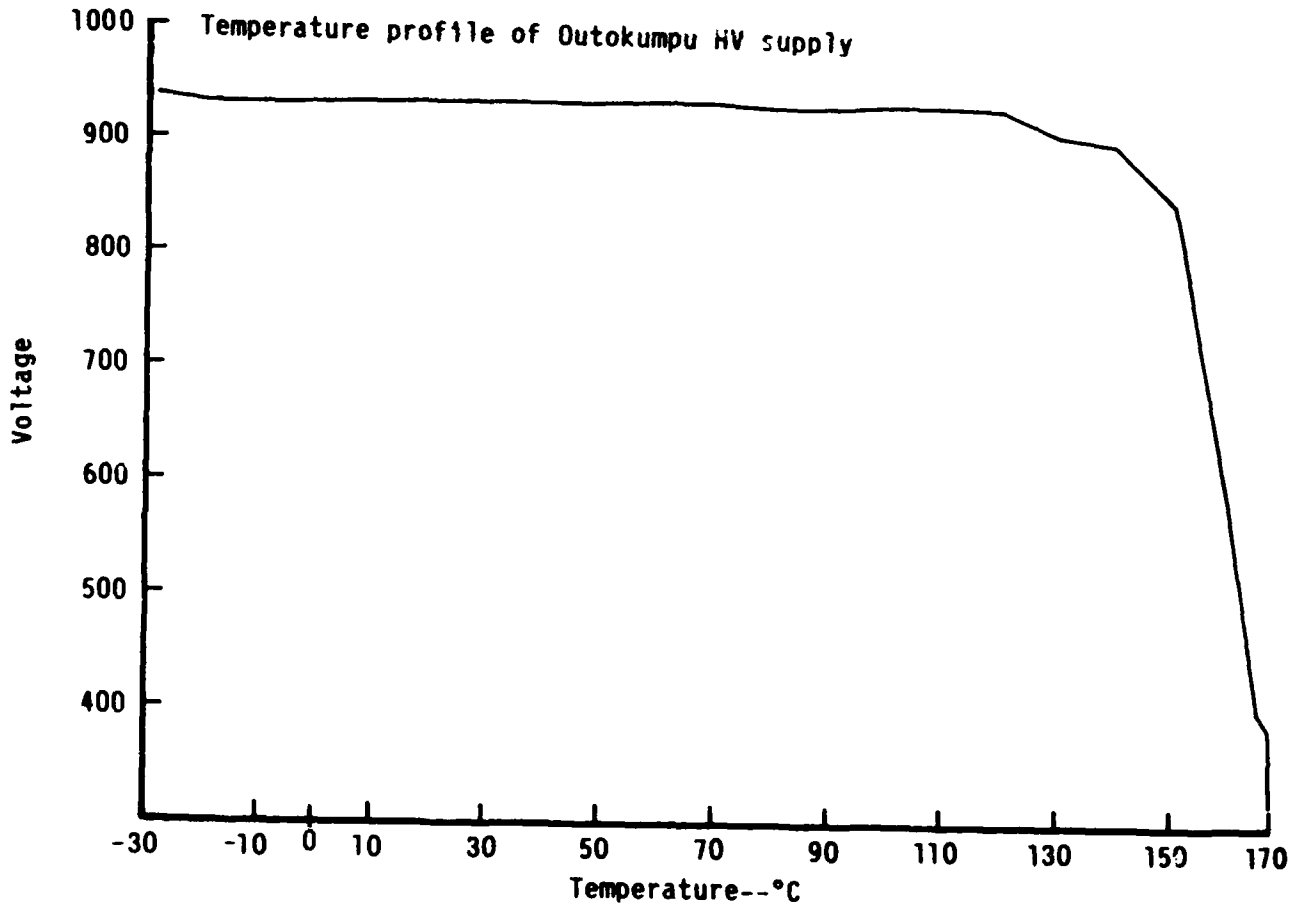
Figure 10. Preamplifier temperature effects.

be analyzed to separate out intermetal effects and background counts. The resulting concentration values can then be supplied to the aircraft mounted engine condition monitoring system through the D/A converter or through the serial data output.



TE88 4829

Figure 11. High voltage power supply schematic.



TE88-4830

Figure 12. High voltage power supply temperature effects.

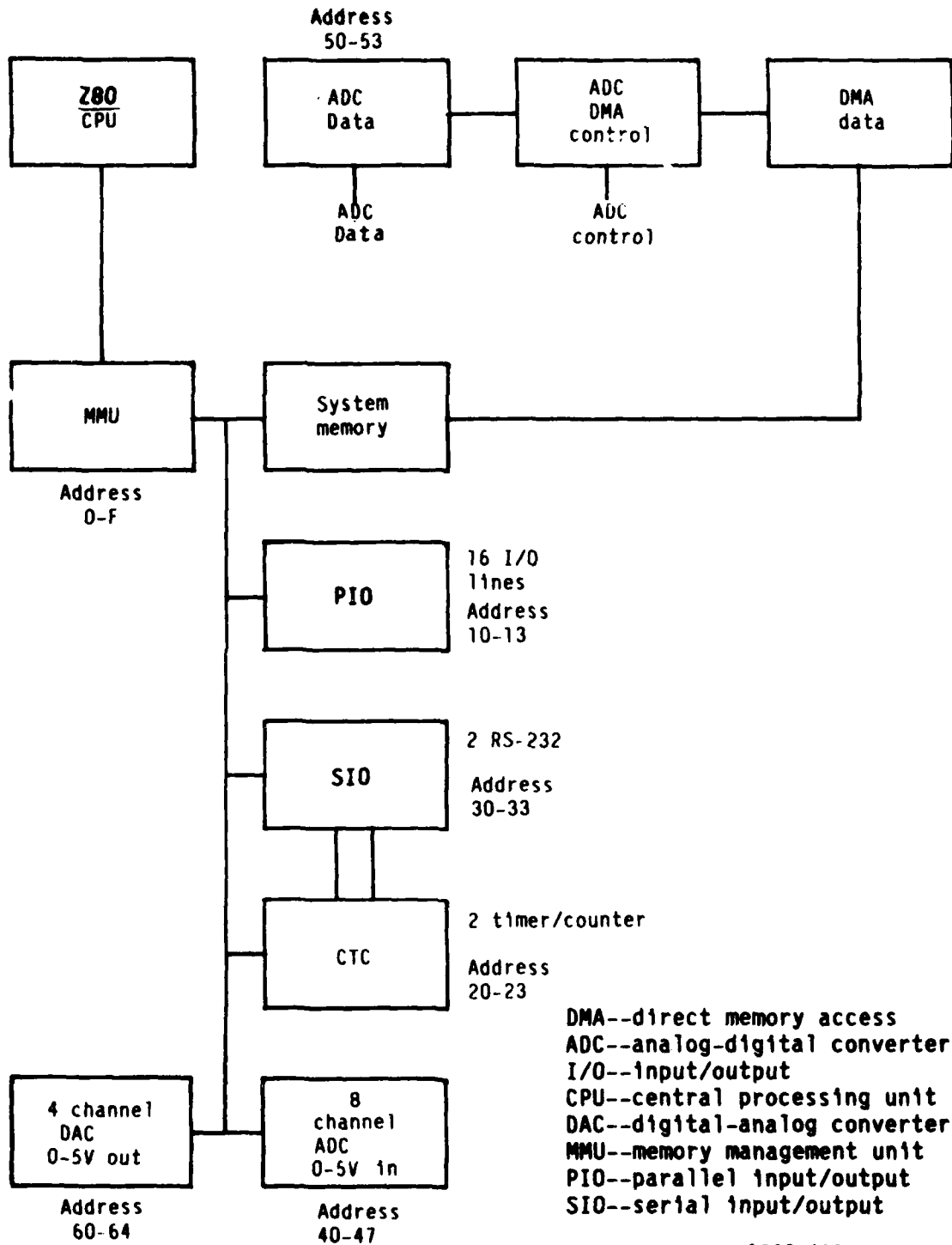


Figure 13. Data processing electronics block diagram.

## V. SENSOR APPLICATION TESTING

This section describes the results of application testing performed to date to determine sensor sensitivity and to reduce background.

### 5.1 INITIAL SENSITIVITY TESTING

This subsection describes the results of preliminary sensitivity testing done in the May-June 1987 time frame. This testing was performed with both a commercial energy dispersive analysis system (PGT M500) and a commercial proportional counter system (X-MET 820). The testing was done on new and used oil samples from Allison Gas Turbine Division and on new oil, a simulated used oil sample, and a 30 ppm standard supplied by the Air Force. In addition, iron in mineral oil standards were prepared at concentrations of 50, 468, and 1000 ppm and analyzed.

Preliminary investigations with a PGT M500 SiLi detector system showed the presence of chromium (Cr), iron (Fe), nickel (Ni), copper (Cu), zinc (Zn), lead (Pb), and molybdenum (Mo) in the 30 ppm standard compared with blank mineral oil. These were measured with an Rh tube at 35 kV, 0.060 mA with a silver filter. The measurement time was 100 sec (live time) with an amplifier time constant of 2 microseconds. Under these conditions the full wave, half modulation (FWHM) at Mn K-alpha was 210 eV. These elements are the principal elements of interest for wear analysis and different conditions were not used to look for other elements.

The detection limit for Fe for these measurement conditions was calculated using the formula:

$$\text{MDL (3-sigma)} = \frac{3}{M} \left( \frac{B}{T} \right)^{1/2}$$

where

- MDL = minimum detectable limit
- M = net counts/sec/unit concentration
- B = background counts/sec
- T = analysis time in seconds

For Fe, the relevant values were:

$$M = \frac{(945-583)/100}{30} = 0.1207$$

$$B = 5.83$$

$$T = 100$$

This gave,

$$\text{MDL}_{\text{Fe}} = 6 \text{ ppm in 100 sec}$$

which corresponds to  $\text{MDL}_{\text{Fe}} = 3.5 \text{ ppm in 300 second}$ . Comparable detection capabilities may be expected for the other elements (Cr, Ni, Cu, Zn, Pb) with the described SiLi detector measurement conditions.

Analysis of the Allison used oil sample showed that Fe, Cu, and Zn were present in the used oil spectrum. Comparison of the Allison used oil versus the blank

oil sample showed Fe, Cu, and Zn were present in the blank spectrum also. These were impurity lines from scatter within the viewing field of the SiLi system. They were not in the blank oil. These impurity lines must be reduced to the lowest possible level in the on-line monitor configuration.

A preliminary fit of the window counts in the SiLi spectrum was made for the 50, 468, and 1000 ppm synthetic standards. The Fe fit was quite encouraging with agreement on the order of the 6 ppm detection limit.

Some preliminary measurements were also made with the X-MET 820 proportional counter system. The 30 ppm standard was measured with a 20 mCi Cm 244 source; the collection time was 300 second. The detector limit under these conditions was:

$$MDL_{Fe} = 10 \text{ ppm in 300 second}$$

which is about a factor of 3 poorer than for the SiLi system.

Similar measurements were made with a 4 mCi Cd109 source, which yielded a similar detection limit of 10 ppm in 300 second.

Initial sensitivity testing showed the need to concentrate in defining proper geometry and measurement conditions for the proportional counter system with a Cm 244 source.

## 5.2 FLOW CELL TESTING

This subsection describes the testing done in the July 1987 - March 1988 time frame with the actual flow cell and efforts to reduce iron background counts.

The main concern of the system design is the reproducible detectability of working trace levels of iron in solution. There were some uncertainties in the reliability of Air Force oil based standards used in the initial testing, and in the initial cell design tests, the results were not consistent. Background scattering was quite high, and iron contamination signals were seen from a variety of sources.

The approach was then taken to reduce system background to minimum attainable levels, then to treat improvement of detectability as a separate problem.

The known difficulty was to reduce the iron signal background to permit 10 ppm levels (and lower) to be detected from the sample in a clean manner.

Iron seems to be almost ubiquitous. For example the original cell design had assumed the use of a 10 mil (0.010 inch) thick beryllium window to the oil, and at the time of the preliminary design review, Allison had pressure tested a full area cell to pressures in excess of 100 psi with a beryllium window.

However even pure grade beryllium foil can contain up to 300 ppm Fe and can significantly affect the system iron background level.

Figure 14 shows the background spectrum from the 0.010 Be window alone. This is the window that was pressure tested at Allison. The very significant iron background signal is clearly unsatisfactory, and can make low level detection of Fe from the oil sample virtually impossible.

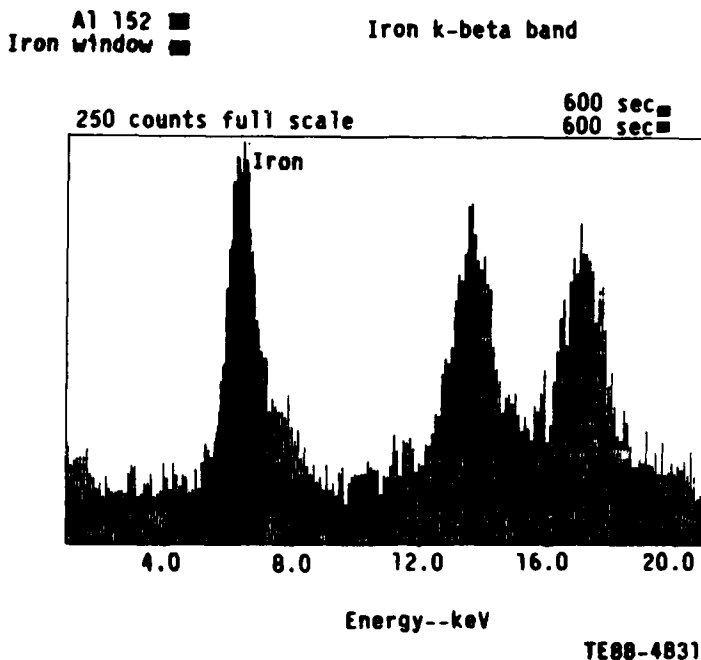


Figure 14. Background spectrum from beryllium foil window.

The intensity of the iron signal is approximately that observed from a 500 ppm Fe standard sample of the type described later.

Figure 15 shows a backscatter spectrum from air (no sample or window) that is of low level and is flat in the region of interest. This represents the inherent background scattering within the cell.

Several alternative window arrangements have been considered including laminated Kapton assemblies with grid supports. The most promising and simplest consists of a 0.010-inch thick polyimide window machined from plate material for strength. It is difficult to machine this much thinner. The windows seem quite strong, but the window has not yet been tested under pressure.

An X-ray fluorescence (XRF) analysis was made of this material and as expected it is totally free from contaminants. The background scattering spectrum using the polyimide window is shown in Figure 16.

With this window the system background is quite low, and at these levels, differing effects of gas mixtures in the proportional counters can now be seen.

These effects are shown in Figure 17 for an analysis of a pure water sample where the (a) spectrum from an Ar-Xe tube is compared with the (b) spectrum from a Ne-Ar gas mixture, which shows almost 50 percent reduction of background level in the region of interest.

These results were only obtained after quite careful design of antiscattering baffles and source holders, and considerable ongoing help from Outokumpu Finland based on their experience in this area with their X-MET products.

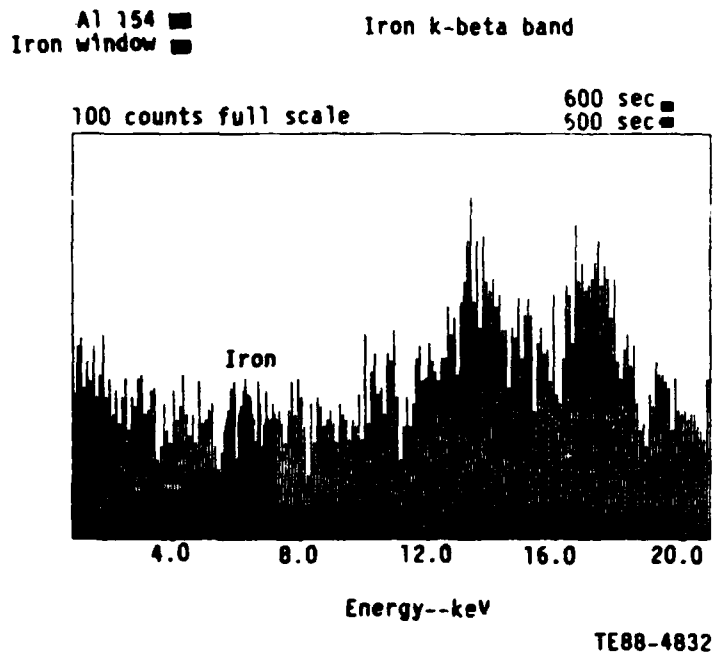


Figure 15. Background spectrum from air.

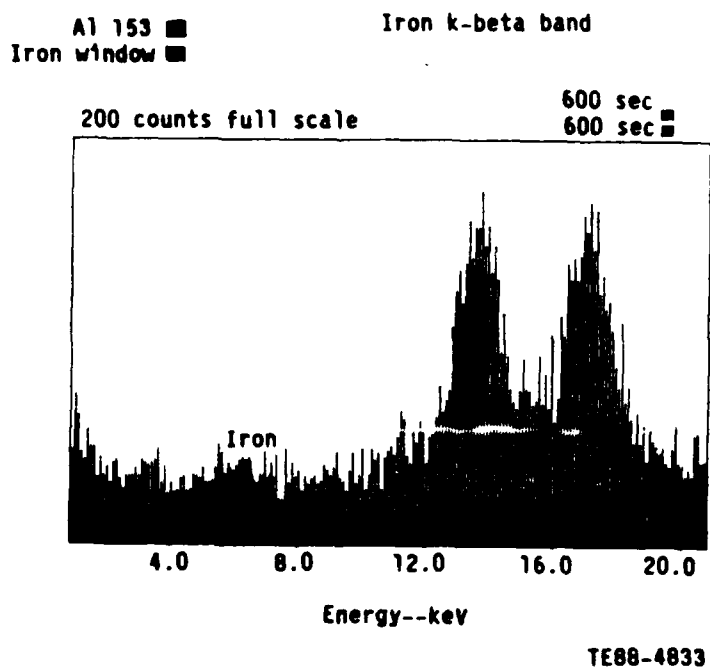
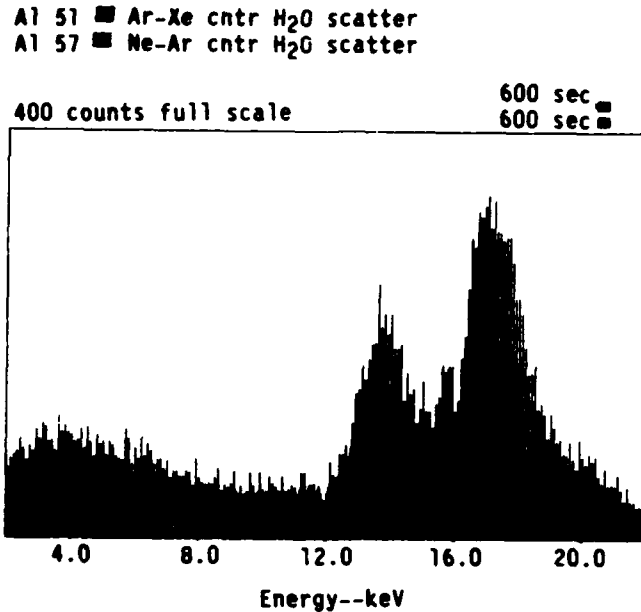


Figure 16. Background spectrum from polyimide window.



TE88-4834

Figure 17. Background spectra argon-xenon and neon-argon detectors.

In addition to the two standard X-MET Type 490 proportional counters used in the initial stages of the project, five special miniature counters have been received from Finland as the project has progressed with different gas mixtures and shielding liner designs (S/N 306, 307, 308, 310, 311).

Later another low background Ne-Ar tube S/N 100 X was received from Finland, designed in an attempt to further reduce the "residual" system background shown in Figure 18. This is an expanded display of the background spectrum taken with a pure water sample and polyimide window. Since the polyimide material is free of contaminants, the residual background must be coming from the system, probably the detector.

There are several factors in proportional counter design that are entering the picture at this level. One, for instance, is the residual iron content of the beryllium entrance window of the proportional counter itself. Other factors are edge shielding of the window, the structure of internal liners, and the uniformity of electric fields to minimize space charge effects in the ionization process.

The S/N 100X design is believed to be about the best that can be achieved as far as high detectability and low background.

To determine the system performance rigorously certified standard Fe solutions obtained from Fisher Company were analyzed. These are water based Fe solutions of nitrate in dilute nitric acid, quite stable and capable of stable dilution to low ppm levels. A series of spectra is shown in Figures 19 through 21 for 600 second live time analyses of samples fabricated from the standard solutions.

Signal from the samples is being seen at the 10 ppm and 20 ppm levels as indicated in Figure 22 and Figure 23 spectra.

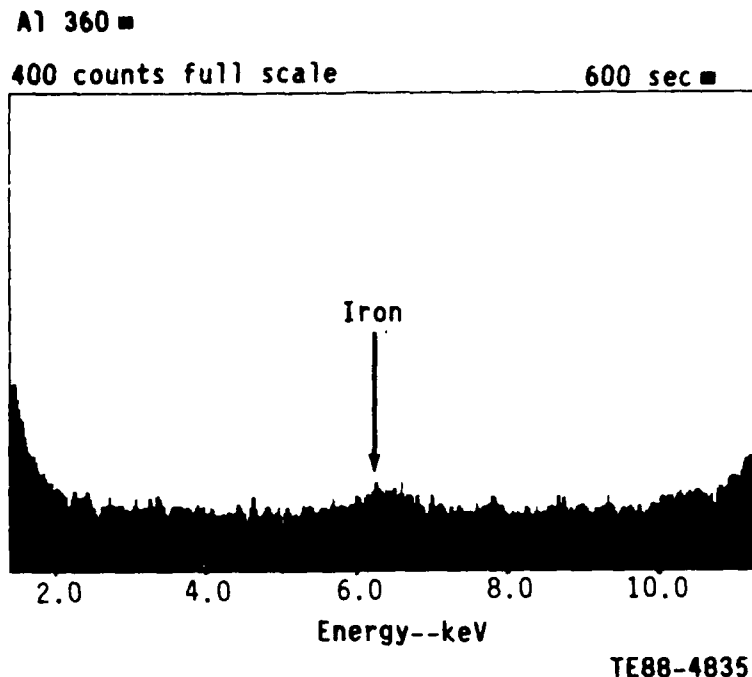


Figure 18. Background spectrum 0 ppm sample, polyimide window.

Figure 24 shows the data and response curve for the system based on 600 second analyses and using the integrated counts from an iron window region defined between 5.6 keV and 7.2 keV. This window region is shown computer shaded in many of the spectra.

The accuracy of analysis is limited by the statistical nature of the data, including the additive error in the background level measurement.

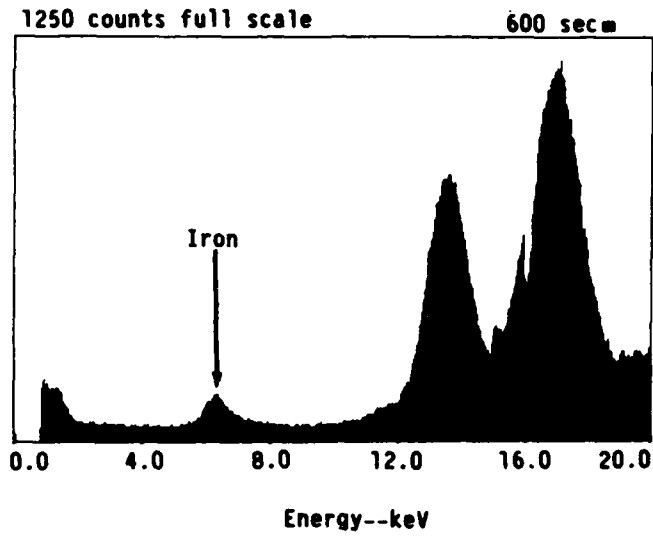
The data in Figure 24 indicate around  $\pm 8.5$  ppm ( $1\sigma$ ) accuracy based on a 600-second analysis of samples and background.

This was not considered quite good enough for this project since the goal was  $\pm 2$  ppm sensitivity; however, the results are considered promising for the following reasons. First, this is a good detectability for a proportional counter system and with the background contamination problems apparently under control the detectability can be improved by increased irradiation of the sample. An increase of up to factor 3 in source strength is available to us with the standard size source capsules. Second, the detectability in water solutions is more difficult than in oil matrix. A comparison of absorption coefficients suggests about 3X improvement in detection sensitivity might be obtained for oils as described in the next section. Repeated data from the Air Force 30 ppm oil standard seem to confirm this. However, a verifiable standards base needs to be used and a series of standards from Conostan have been obtained for testing with MIL-L-7808 and MIL-L-23699 oil.

### 5.3 DETECTABILITY LIMITS IN WATER AND OIL

Differences in minimum detectable limits (MDL) for Fe in water versus oil matrixes have been investigated. This was to clarify apparent discrepancies between current MDLs with Fisher aqueous Fe standards compared with previous data with Chemplex Fe in oil standards.

AL365 ■



TE88-4836

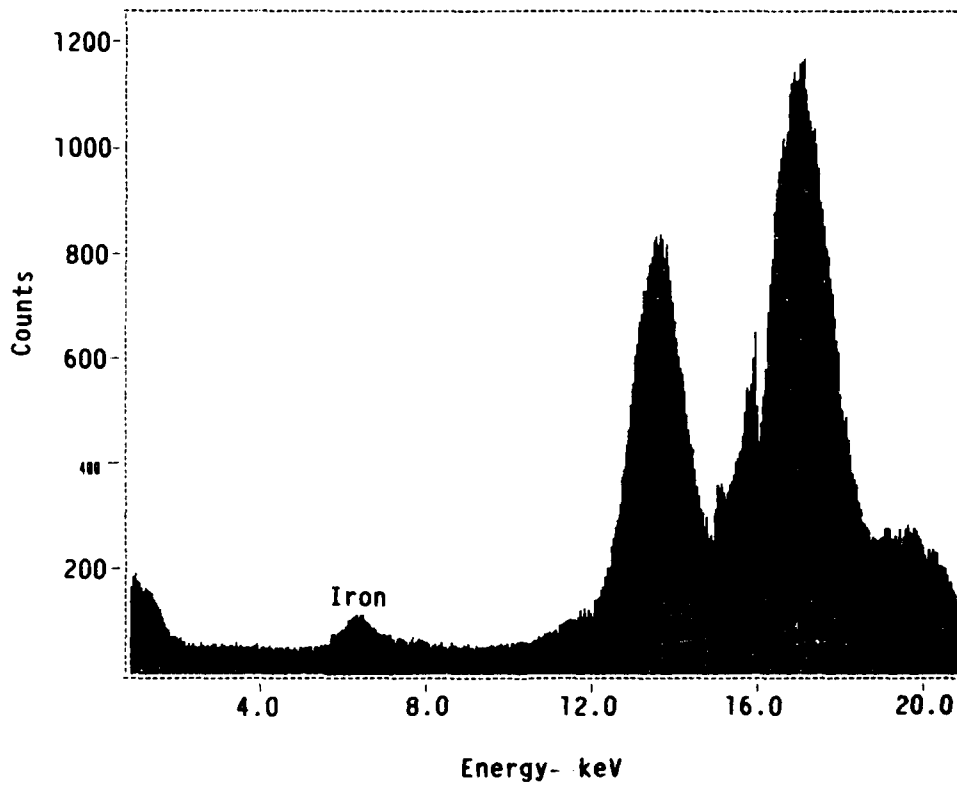
Figure 19. Spectrum 200 ppm iron sample.

Spectrum label

■

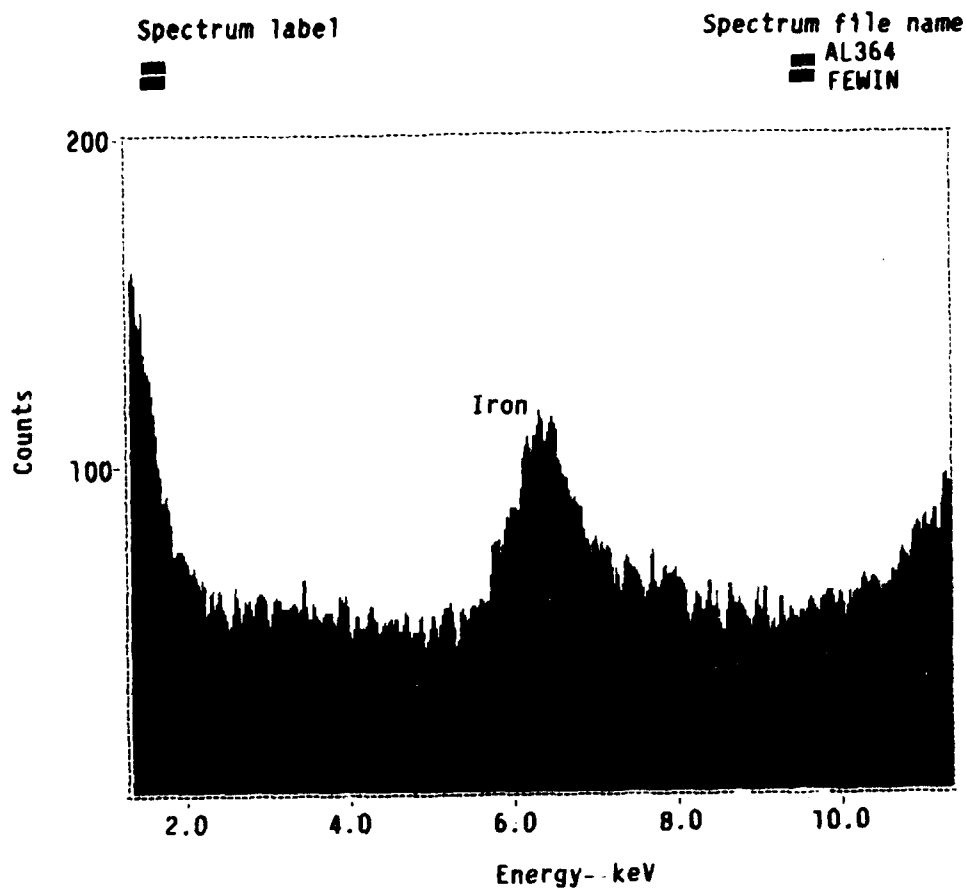
Spectrum file name

■ AL364  
■ FEWIN



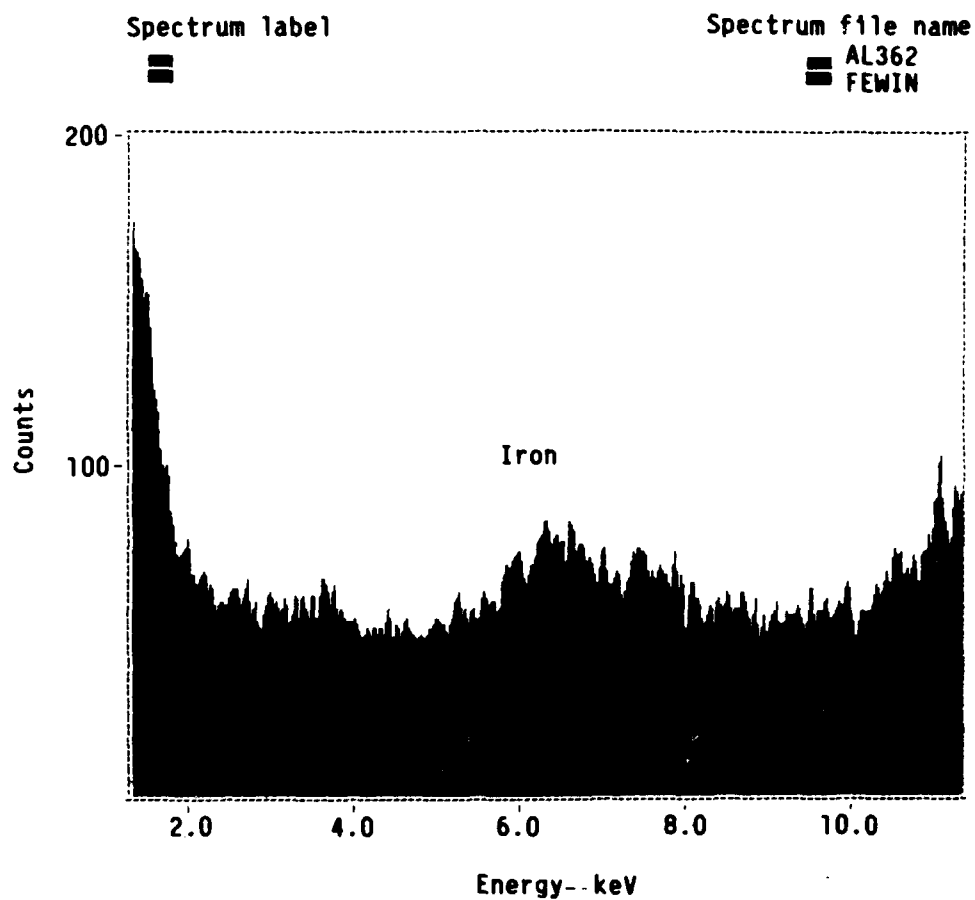
TE88-4837

Figure 20. Spectra 100 ppm iron sample.



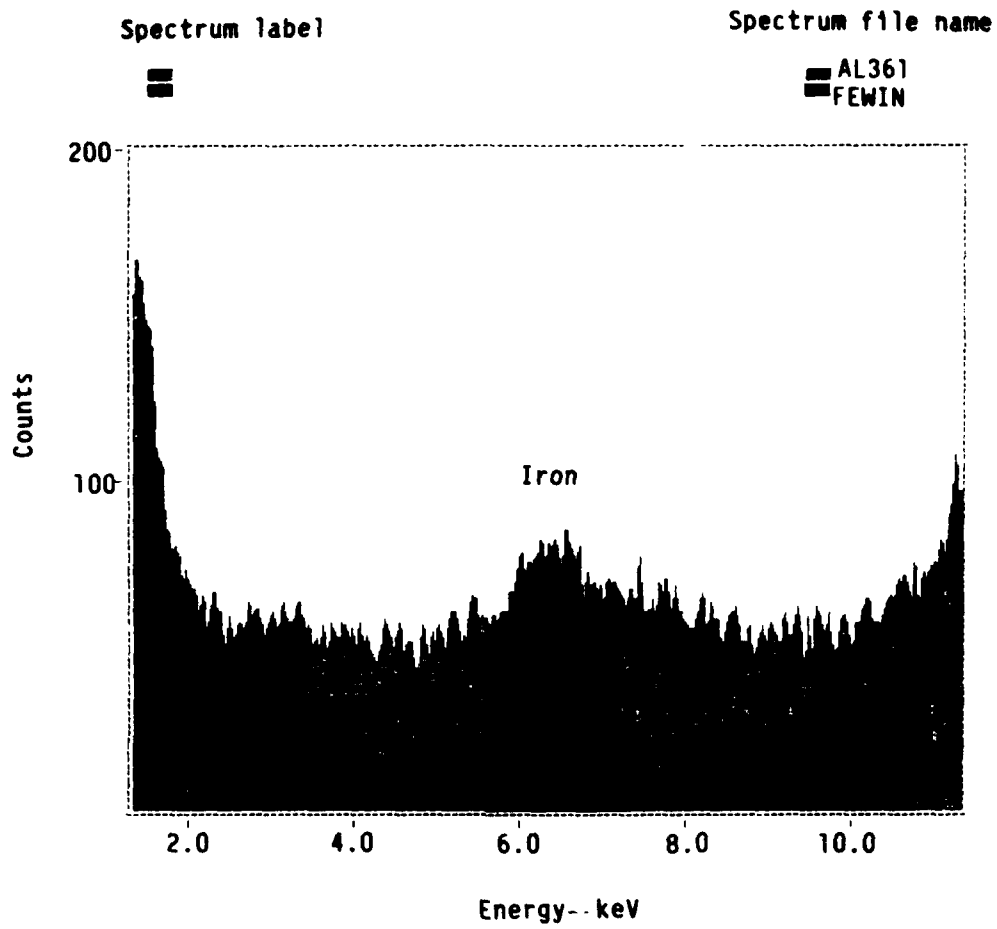
TE88-4838

Figure 21. Expanded spectrum 100 ppm sample.



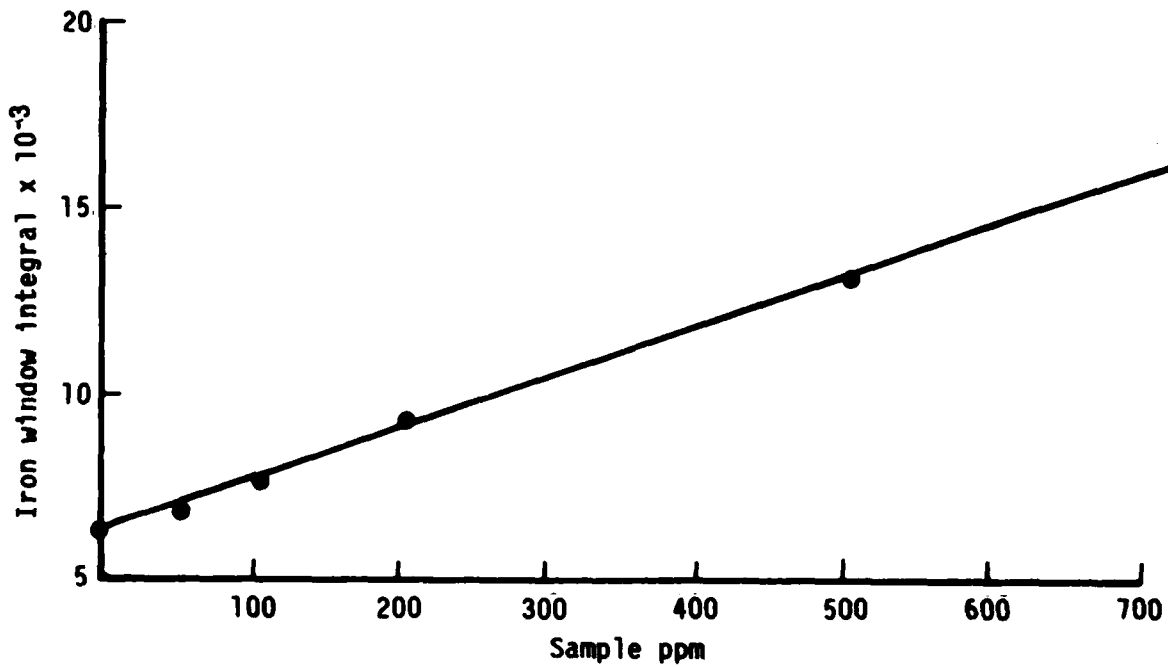
TE88-4839

Figure 22. Spectra 10 ppm Fe sample.



TE88-4840

Figure 23. Spectra 20 ppm Fe sample.



600-sec analysis				
<u>Run</u>	<u>Sample ppm</u>	<u>Fe window integral</u>	<u>Baseline subtract</u>	<u>Analysis ppm</u>
AL126	0	6,383 ± 80	0	
AL128	1,000	20,184	13,801	1,000 norm 13.8/ppm
AL127	10	6,502	119	8.6 ± 8.2
AL129	20	6,697	314	22.7 ± 8.3
AL130	50	6,856	493	36 ± 8.3
AL131	100	7,611	1,228	89 ± 8.6
AL134	200	9,233	2,850	206 ± 9
AL132	500	13,018	6,635	480 ± 10
AL133	750	16,412	10,029	727 ± 11

TE88-4841

Figure 24. Data and response curve--polyimide window.

For purposes of this discussion, the 2-sigma MDL is defined as follows:

MDL(2-sigma) = the concentration with a net intensity equal to two times the standard deviation of background counts

$$= \left(\frac{2}{M}\right) \left(\frac{B}{T}\right)^{1/2}$$

where

M = (net counts/sec)/(concentration)

B = background counts/sec

T = time (seconds)

Based on this, the MDLs for 600-sec measurements, shown in Table 1, have been obtained:

---

Table 1.  
MDLs for 600-sec measurements.

<u>Standard</u>	<u>Matrix</u>	<u>MDL (ppm)</u>	<u>Hardware</u>
Fisher	Water	13	XMET820
Fisher	Water	13	Allison
Air Force	Oil	3	XMET820
Chemplex	Oil	5	XMET820

---

These suggest that the MDL for Fe in oil is 3 to 4 times better than that in water. This is supported by infinite thickness (99 percent) calculations that predict 1.6 mm for water and 6.2 mm for Fe in oil. The latter means that approximately 4 times more volume is observed in an oil matrix provided there are no geometrical constraints. It follows that about 4 times more mass will be measured for the same concentration of Fe in oil compared with that for water. Finally, the ratio of mass absorption coefficients for Fe in oil to Fe in water is about 0.3, which means Fe is reabsorbed three times more by water than oil.

The bottom line is that it now appears reasonable to expect the detection limit for Fe to be a factor of three better in oil than in water. This will be verified with additional measurements to be made with oil standards from Chemplex and Conostan.

#### 5.4 BERYLLIUM WINDOW CONTAMINATION

While rechecking the details of the beryllium window contamination (Figure 14) another 0.010 Be window extracted from an old cell in some other equipment was tested. This window showed a considerably cleaner spectrum and Figure 25 shows the overlaid background spectra obtained from the two foils.

Both foils were standard Be disks obtained from Brush Wellman. The difference is quite high and was totally unexpected.

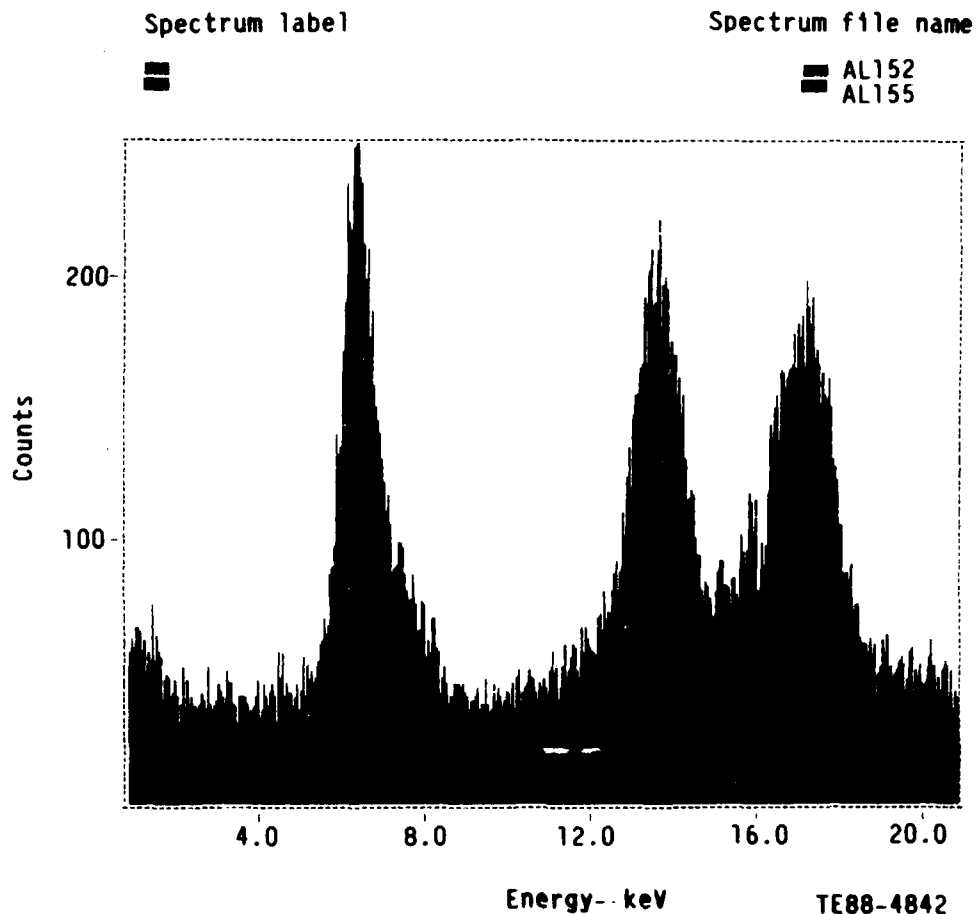


Figure 25. Backscatter spectra from beryllium foils.

Initial indications are that the original cell window was perhaps a very poor specimen of beryllium material and that effort in developing the polyimide window system was unnecessary.

Either the "dirty" beryllium is atypical or else the "clean" beryllium window is exceptionally good. Beryllium is known to contain Fe and other contaminants. Normal pure grade foil can be as high as 700 ppm in Fe and ultrapure PF-10 grade can be as high as 300 ppm. Manufacturers data are shown in Figure 26. This needs to be investigated further with other foils.

It appears possible to select commercial Be window material low enough in background contaminants to come very close to the quality of polyimide material in this application, and polyimide is always a viable backup.

Figure 27 shows an overlay of spectra taken with a pure water sample using the "clean" beryllium window and the polyimide window (dark shaded printout) in the Allison cell.

The polyimide window is better, but not significantly so, and the Be window has the advantage of higher transmission.

An empirical determination of the transmissions at 6.4 keV Fe energy was made by analysis of a 1000 ppm Fe standard solution in a sample cup with 1/4 mil

# BRUSHWELLMAN

ENGINEERED MATERIALS

Brush Wellman Inc • Elmore Ohio 43416 • Phone 419 862-2745 • TWX 810/490-2300

TENTATIVE  
SPECIFICATION

## PF-60 Beryllium Foil

12/17/79

### 1. SCOPE

1.1 This specification defines the requirements for beryllium foil produced by hot rolling hot pressed block and is designated PF-60

### 2. COMPOSITION

2.1 Foil to this specification is produced by rolling hot pressed block with the following chemistry composition:

Beryllium Assay	% Min	99.0
Beryllium Oxide	% Max	0.8
Aluminum	% Max	0.05
Boron	% Max	0.0003
Cadmium	% Max	0.0002
Calcium	% Max	0.01
Carbon	% Max	0.07
Chromium	% Max	0.01
Cobalt	% Max	0.001
Copper	% Max	0.010
→ Iron	% Max	0.07
Lead	% Max	0.002
Lithium	% Max	0.0003
Magnesium	% Max	0.050
Manganese	% Max	0.012
Molybdenum	% Max	0.002
Nickel	% Max	0.02
Nitrogen	% Max	0.04
Silicon	% Max	0.04
Silver	% Max	0.0010

Other metallic impurities (0.04% max. each) as determined by normal spectrographic techniques

2.2 Detailed analytical procedures used by Brush Wellman Inc. are available upon request

TE88-4843

Figure 26. Beryllium foil data sheet (part 1 of 2).

# BRUSHWELLMAN

ENGINEERED MATERIALS

Brush Wellman Inc • Elmore Ohio 43416 • Phone 419/862-2745 • TWX 810/490-2300

TENTATIVE  
SPECIFICATION

## High Purity Beryllium Foil Grade PF-10

12/28/88

### 1. SCOPE

This specification defines the requirements for beryllium foil with 99.4% minimum beryllium content and 0.16% maximum metallic impurity content produced by hot rolling powder-derived billets. It is designated PF-10.

### 2. CHEMICAL COMPOSITION

The beryllium billet used for hot rolling of foil to this specification shall meet the following chemical limits.

Beryllium Content (included Be content of BeO)	99.4% minimum, by difference
Beryllium Oxide	0.6% maximum
Carbon	300 ppm maximum
Iron	300 ppm maximum
Nickel	200 ppm maximum
Calcium	200 ppm maximum
Silicon	200 ppm maximum
Aluminum	100 ppm maximum
Zinc	100 ppm maximum
Magnesium	80 ppm maximum
Copper	50 ppm maximum
Manganese	30 ppm maximum
Chromium	25 ppm maximum
Molybdenum	10 ppm maximum
Titanium	10 ppm maximum
Cobalt	5 ppm maximum
Lead	5 ppm maximum
Silver	5 ppm maximum
Boron	3 ppm maximum
Cadmium	2 ppm maximum

Any other metallic impurity as determined by normal emission spectrography 100 ppm maximum.

TE88-4844

Figure 26. Beryllium foil data sheet (part 2 of 2).

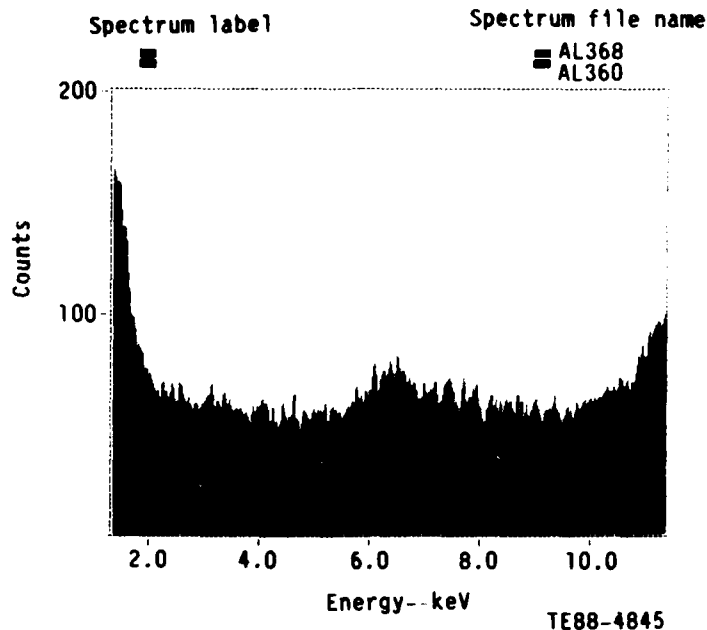


Figure 27. Spectra of clean beryllium compared with polyimide window.

polypropylene foil, then inserting the polyimide window and beryllium window in comparative measurements of iron window intensity, correcting for their slightly different backscatter yields.

On this basis the polyimide window transmission was 56.3 percent versus 79.4 percent for the beryllium foil. This factor 1.41 increase in transmission is important, equivalent to a 40 percent increase in source strength, and improves detection sensitivity.

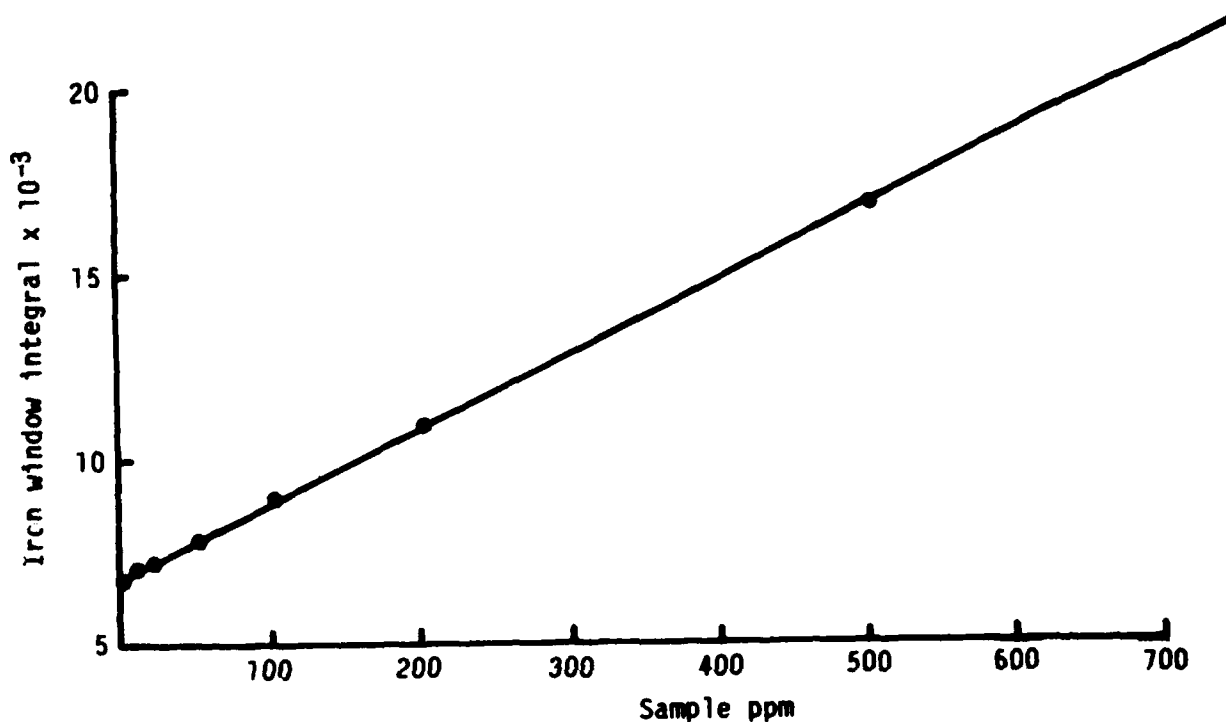
All the Fe standard water based samples have been rerun with the clean Be window on the Allison cell. The spectra shown in Figures 19 through 21 include some of the latest data printouts.

The spectrum plots do not differ significantly in appearance from the polyimide window data, but the response curve data, as shown in Figure 28, are different, and detection sensitivity has improved.

The statistical accuracy based on single analysis for 600 second of background (water) and samples in the 10 ppm to 50 ppm range is now around 6 ppm (6.1) versus around 8 ppm (8.3) of the Figure 24 data of this report.

The MDL, as defined in subsection 5.3, is now improved from 13 ppm to around 8.3 ppm for water matrix samples.

The rationale regarding 3X better detectability with oils is still valid, so the detection goal for the system is now close to being achieved and the increase of source strength as an option for further increase in detection sensitivity is still available.



600-sec analysis

<u>Run</u>	<u>Sample ppm</u>	<u>Fe window integral</u>	<u>Baseline subtract</u>	<u>Analysis ppm</u>
AL159	0	6,844 ± 83	0	
AL168	0	6,895 ± 83	0	
AL158	1,000	26,526	19,656	1,000 norm 19.65/ppm
AL161	20	7,269	399	20.3 ± 6.0
AL162	10	7,210	340	17.3 ± 6.0
AL163	50	7,999	1,129	57.4 ± 6.2
AL164	100	8,991	2,121	108 ± 6.4
AL165	200	10,922	4,052	206 ± 6.8
AL166	500	16,859	9,989	508 ± 7.8
AL167	750	22,016	15,146	770 ± 8.6
AL169	10	7,168	298	15 ± 6.0

TE88-4846

Figure 28 Data and response curve--clean beryllium window.

## VI. SENSOR VIBRATION TESTING

This section describes the results of vibration testing performed on the sensor portion of the in-line wear monitor system. The testing was performed at Allison from 2 May through 5 May 1988.

### 6.1 SENSOR MOUNTING

The sensor flow cell was designed to fit on the TF41 engine in place of a tube going from the oil tank to the oil pump inlet. This location was picked from a viewpoint of ease of insertion, low pressure, full oil flow ahead of the oil filter, and some vibration isolation due to O-ring suspension of the pipe. In discussions with engine designers in connection with the vibration testing, it was discovered that the oil tank is hard mounted to a support tray that connects to the internal engine frame and could be a bad vibration point. There are no actual vibration profiles of this point in the engine. Accelerometer readings are to be taken at Allison in August 1988 at this location on an instrumented flow cell during a TF41 endurance test. Alternative materials, tube thicknesses, and mounting schemes were also discussed. However, program time and funding limitations dictated that effort be concentrated on making the existing design operate under vibration conditions at least comparable with standard engine component profiles. Toward that end, vibration problem areas in the sensor are to be explored with a view to next step improvements until a limit is reached with the existing mounting. Beyond that point changes to engine mounting methods to improve vibration isolation of the entire flow cell will be needed.

### 6.2 VIBRATION TEST RESULTS

Rather than attempting to analyze ppm Fe levels in oil, which would have been premature, the cell was fitted with a copper disk window.

This gave a strong copper X-ray line from the sensor and the X-ray spectra enabled observation of system resolution, peak stability, and background levels.

A spectrum from the sensor is shown in Figure 29.

Spectra were obtained using a PGT system 3 analyzer with floppy disk storage.

The shake table equipment consisted of a large Thermotron environmental chamber vibrator driven by a Spectral Dynamics computer-based controller system.

In the report, reference is made to vertical, lateral, and axial vibration tests. This relates to the mounting orientation of the sensor on the shake table as shown in Figure 30.

#### 6.2.1 Test I--Frequency Scans

The sensor was mounted between steel blocks simulating the engine mounting knuckles with the double O-rings on the end pipe sections.

The assembly was suspended in a yoke that was bolted to the shake table. The mounting scheme could be modified to permit vibration in vertical, lateral, and axial orientations as defined previously.



A 1/2 g sinewave scan was performed up to 3 kHz at a fairly slow rate (1 octave/minute) and sensor resonances were detected by accelerometers mounted to the electronics compartment.

The output baseline noise from the data channel amplifier in the sensor was monitored with an oscilloscope. Baseline level resonances in the electronics generally seemed to correlate with the mechanical resonances, as expected, although some strong mechanical resonances had very little effect on sensor output. The observed electronic resonance frequencies were then reexamined and X-ray spectra from the sensor taken at these bad spots, holding the shake table at resonant frequency.

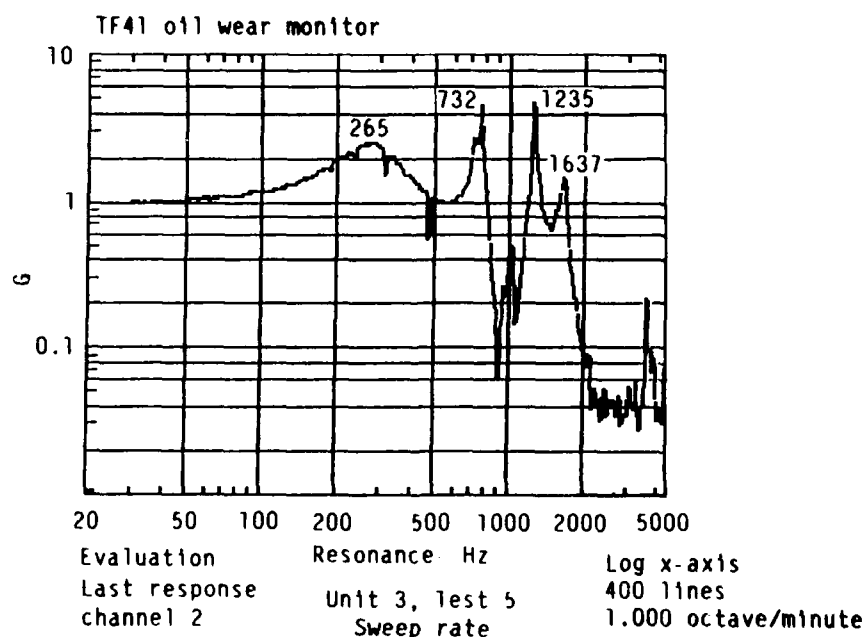
#### 6.2.1.1 Vertical Vibration Scans

Figure 31 shows the sensor resonance profile with a broad resonance at 265 Hz (2.3 g), 3.5 g sharper resonances at 732 and 1235 Hz, and a 1.6 g resonance at 1637 Hz.

Spectrum A1 207, Figure 32, at the 265 Hz resonance shows the sensor is operating normally, with some low level noise introduced.

Spectrum A1 208, Figure 33, at the 732-5 Hz resonance shows however that the sensor response is wiped out by the introduction of a substantial noise slope entering the spectrum from low energies. The location and analysis of the copper peak remained intact so the gain stability and operation of the sensor is not being affected; background noise pulses are being injected into the analysis.

This was the worst spectrum obtained in these results.



TE88-4849

Figure 31. Resonance profile--vertical vibration sweep.

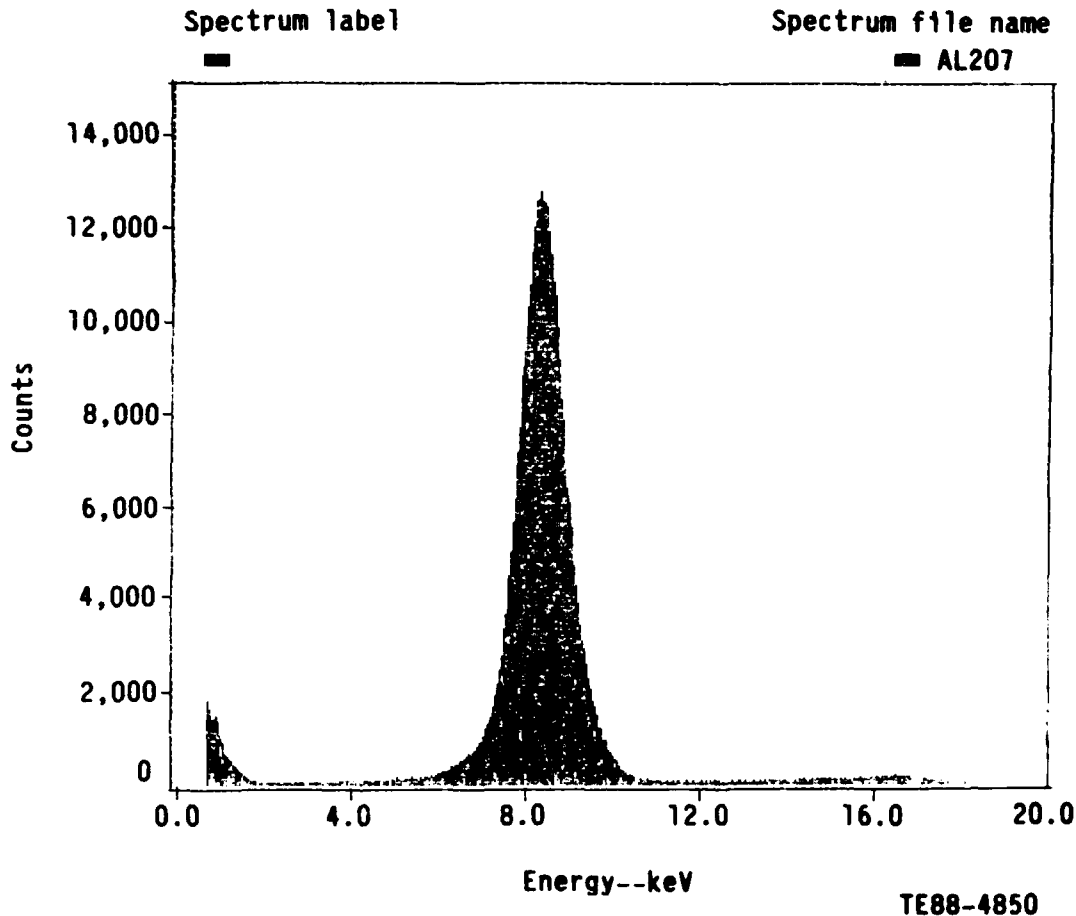


Figure 32. Spectrum at 265 Hz resonance.

Spectrum Al 207, Figure 34, taken at the equally strong 1235 Hz resonance shows no such problem.

Similarly spectrum Al 210, Figure 35, at the 1637 Hz resonance shows the sensor performing X-ray analysis properly.

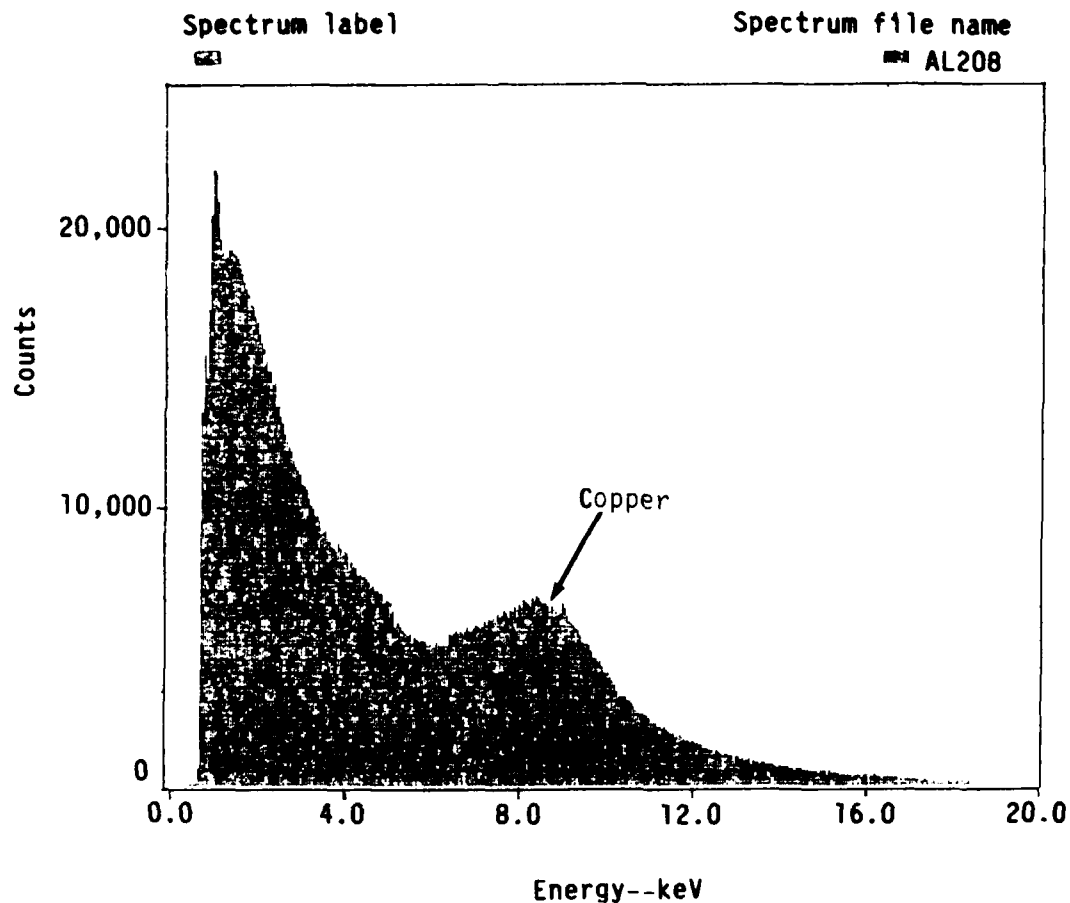
#### 6.2.1.2 Lateral Vibration Scan

Figure 36 shows the response of the sensor to lateral vibration sweep.

The general profile is similar to the vertical response (Figure 31) in having two resonance peaks centered around 1 kHz, although there is no equivalent to the 1637 Hz resonance, and the lower component below 500 Hz is different. Spectra at the 763 Hz and 1238 Hz resonances showed no problem with analysis.

#### 6.2.1.3 Axial Vibration Scan

The mechanical resonance profile is shown in Figure 37. Once again the profile is similar to the other axes in showing resonance peaks each side of 1 kHz, although the low frequency profile is different.



TE88-4851

Figure 33. Spectrum at 732 Hz resonance.

The lower frequency components might be attributed to the table mounting assembly (no baseplate mounting profiles were taken) and the consistent double peak resonance structure to the cell and sensor.

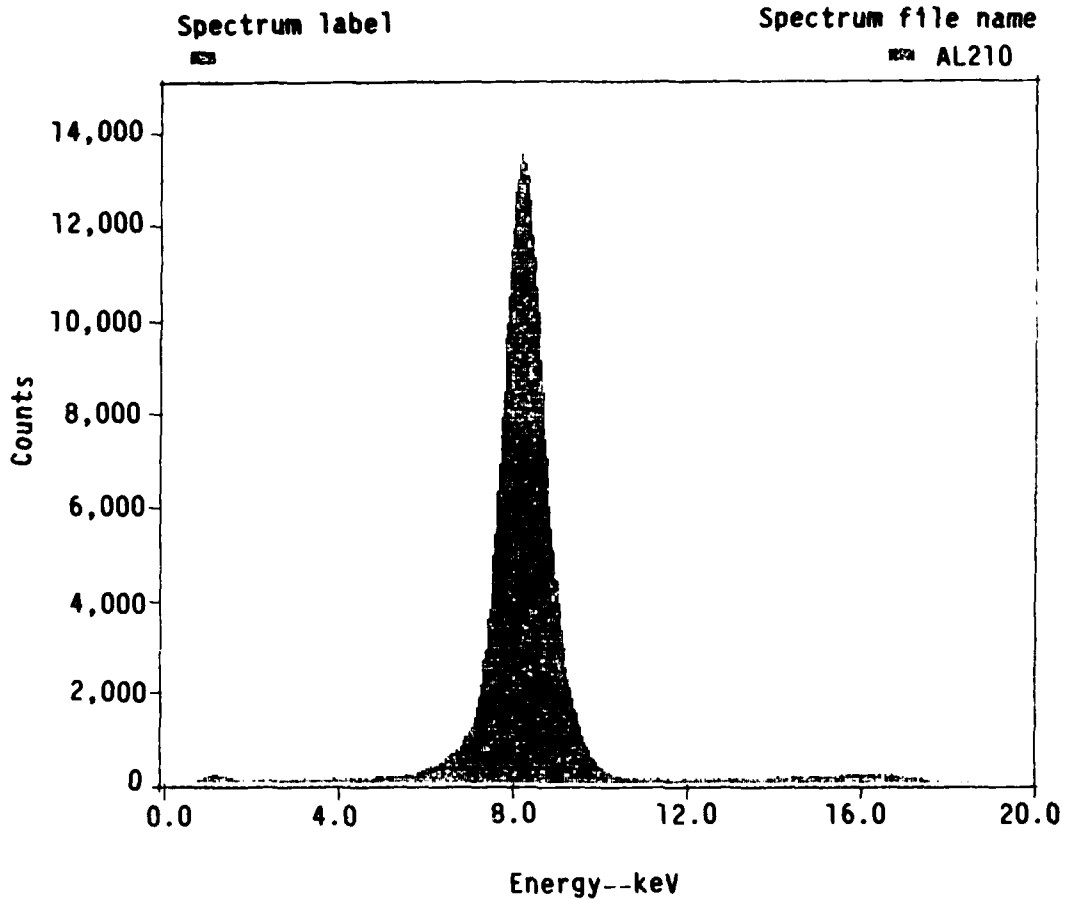
The relatively small resonance at 625 Hz had a marked effect on sensor baseline output and consequently on the analyzed spectrum as shown in A1 214, Figure 38.

The larger resonance at 1187 Hz (1.7 G peak) was handled all right by the sensor as shown in spectrum A1 215, Figure 39.

The apparent shift of the copper X-ray peak from its correct energy at 9 keV in the spectrum A1 214, Figure 38, was due to an incorrect dial setting of HV bias on the counter and is not a system fault.

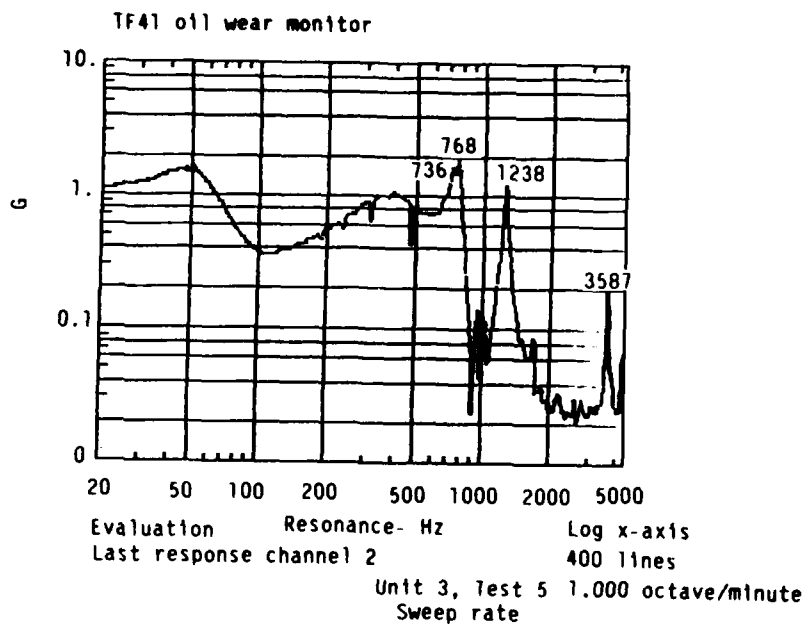
The voltage correction (from 548 V to 546 V) was made for the spectrum A1 215, Figure 39.





TE88-4853

Figure 35. Spectrum at 1637 Hz resonance.



TE88-4854

Figure 36. Resonance profile--lateral vibration sweep.

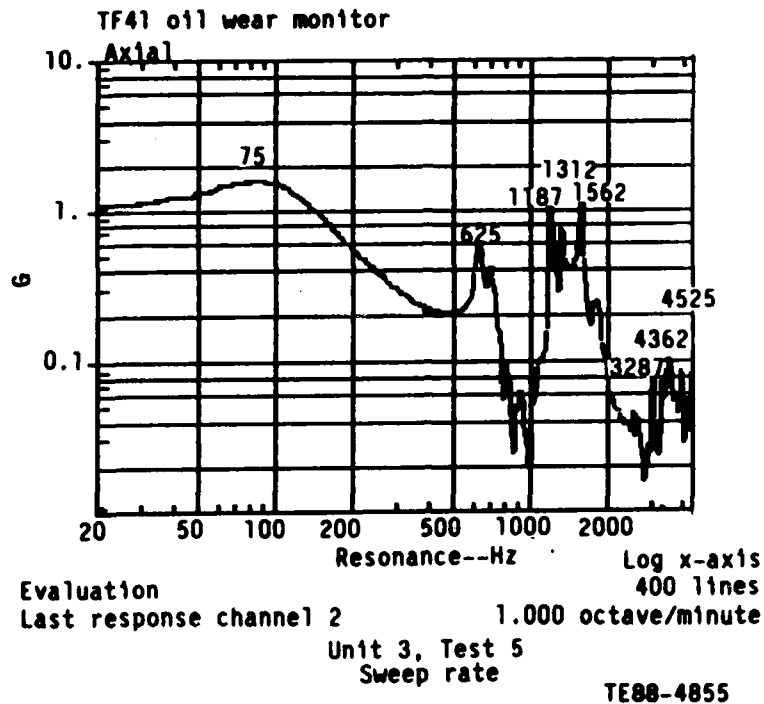


Figure 37. Resonance profile--axial vibration sweep.

Spectrum label Spectrum file name  
 AL214

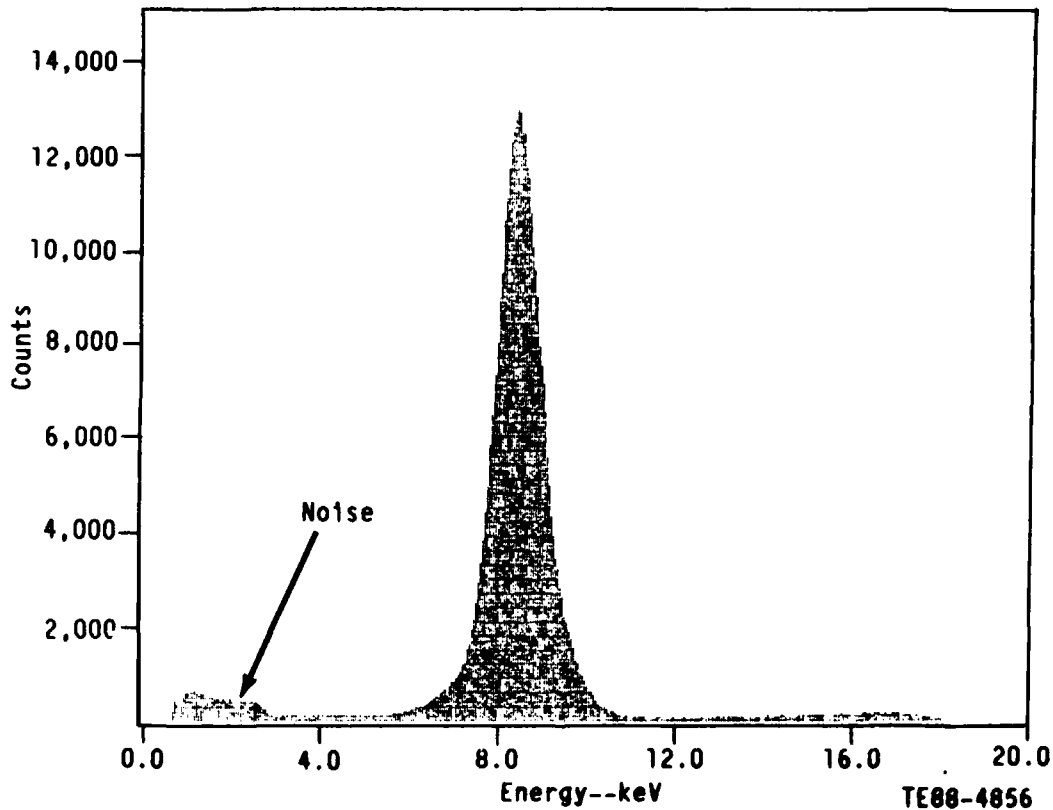


Figure 38. Spectrum at 625 Hz resonance.

Spectrum label

Spectrum file name

AL215

AL215

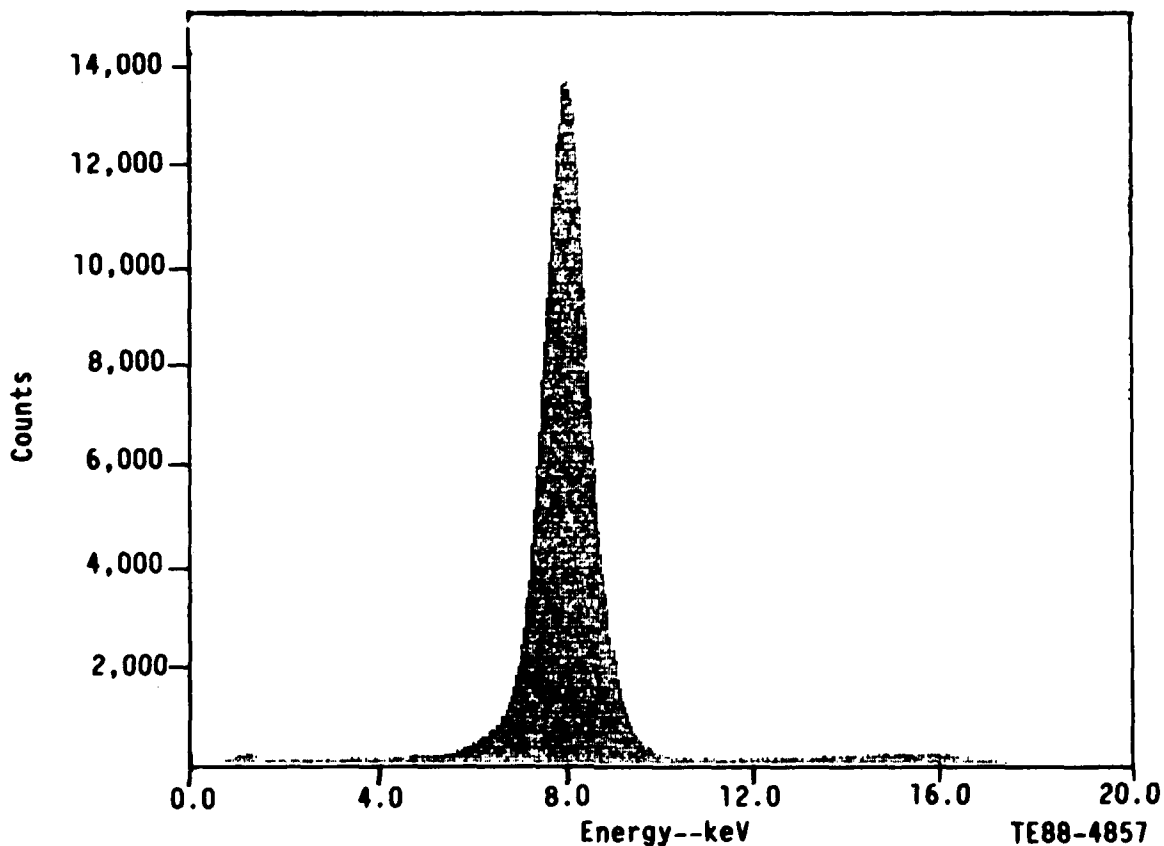


Figure 39. Spectrum at 1187 Hz resonance.

The copper foil was removed from the cell. Since the analysis "sample" was now not present, a test pulser was connected to the system. Provision already existed in the design for test pulse injection through the counter.

Figure 40 shows the Al 217 spectrum for the pulser. There are two pulser lines due to electronic pulse shaping. The spectrum also shows iron background from deep scattering in the stainless steel cell as shown by the expanded spectrum Al 217b in Figure 40.

The sensor was remounted to the shake table and frequency scanned in the vertical axis. The response profile is shown in Figure 41.

The 712.5 Hz resonance had a major effect on the sensors baseline signal, and a spectrum taken at this resonance (Al 218, Figure 42) shows the pulser resolution is destroyed into multiple split peaks and the background noise submerges the Fe peak seen in Figure 40.

The pulser resolution was also badly degraded, though not so drastically, at a lateral vibration resonance at 701 Hz (spectrum Al 219, Figure 44).

This indicated the copper foil window was not the vibration culprit. Also since the pulser treats the counter as an injection capacitance, the loss of

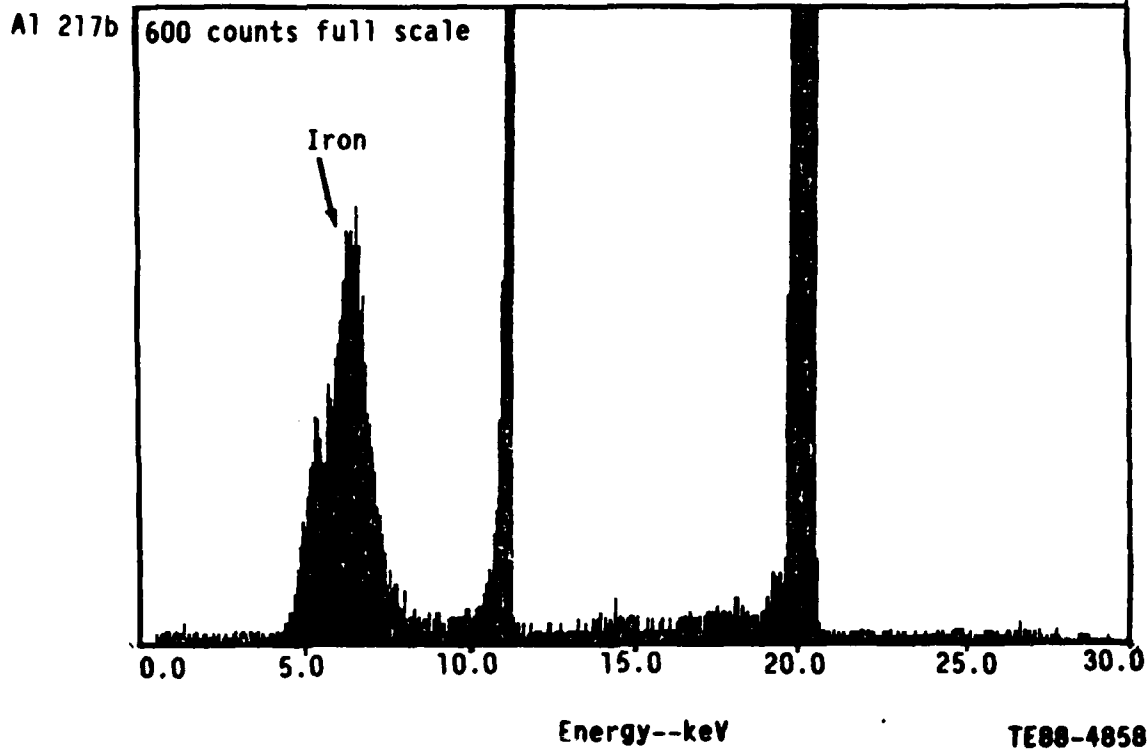
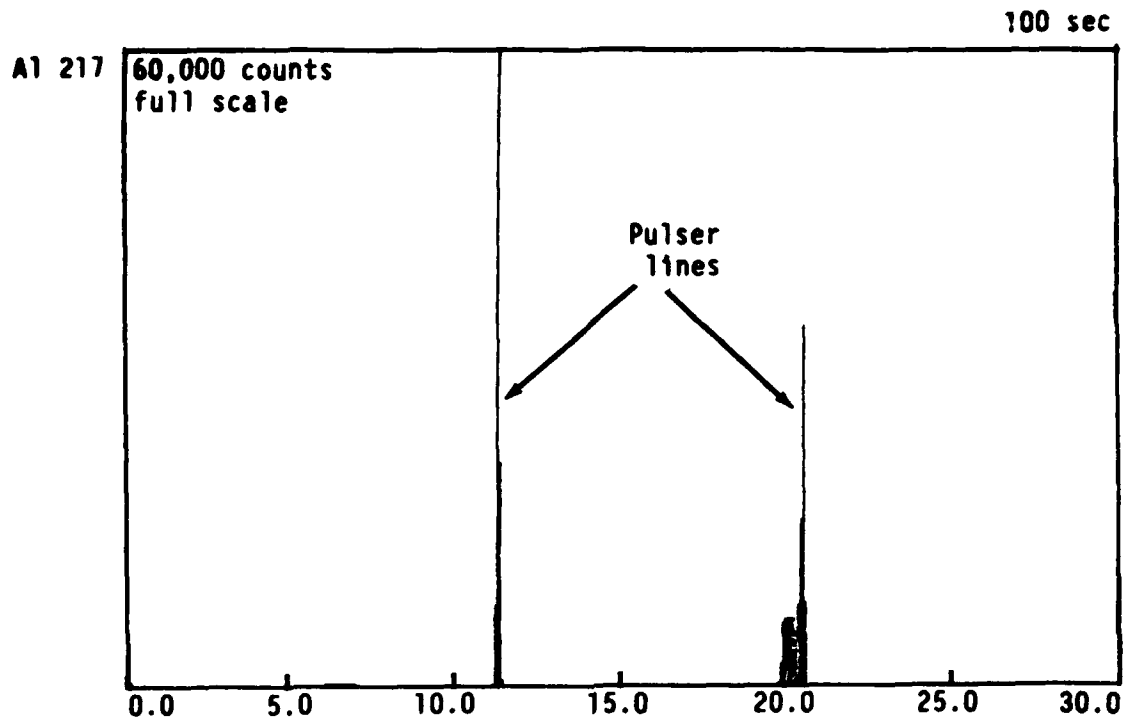


Figure 40. Spectrum with test pulses into sensor copper foil window removed.

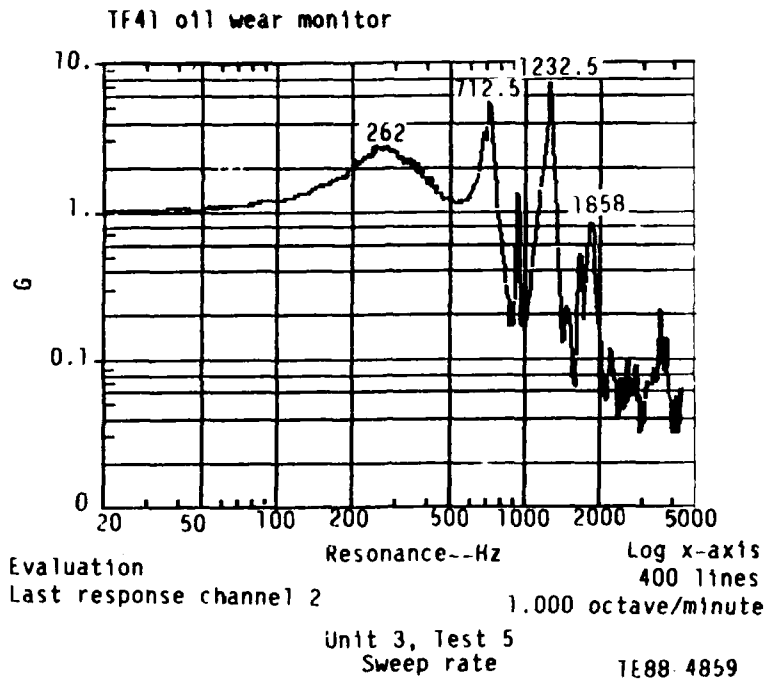


Figure 41. Resonance profile--vertical vibration sweep no cell window.

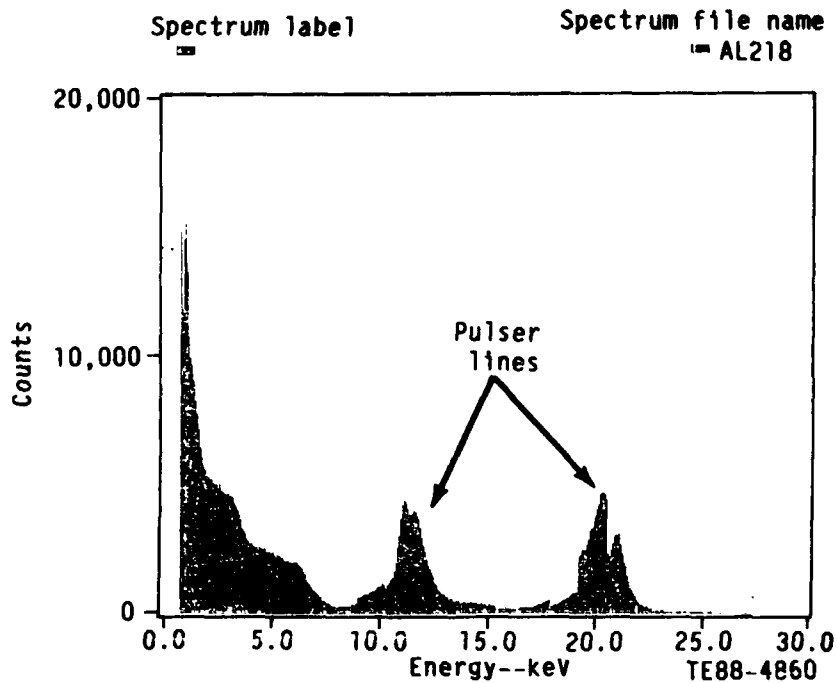


Figure 42. Spectrum at 712.5 Hz resonance.

system resolution was indicated as being primarily an electronics problem, unrelated to the X-ray pulse production process.

In this case the effect would be independent of HV bias on the counter. The HV was turned down and spectrum Al 220 (Figure 43) acquired at the fixed 701 Hz lateral resonance.

Comparison of spectra Al 219 (with HV bias) and Al 220 (zero HV bias) in Figure 43 shows the effect is still present even at 0 V HV, although perhaps a little less severe.

Figure 44 shows a vertical scale expansion. The Fe X-ray peak is absent in spectrum Al 220 as the counter HV bias is zero and no X-ray pulses are produced.

Since the problem was therefore electronic and the electronic boards were not potted or conformally coated, the next possibility was electronic component vibration.

The sensor was removed, opened up, and circuit boards were conformally coated by a thick covering of Dow Corning 3140 room temperature vulcanizing (RTV) coating, using Dow Corning No. 1204 primer.

Although the coating had not entirely set overnight, the cell was reassembled with copper foil window and resubmitted to a vertical vibration scan. The pulser was also coupled into the system.

The resonance profile is shown in Figure 45.

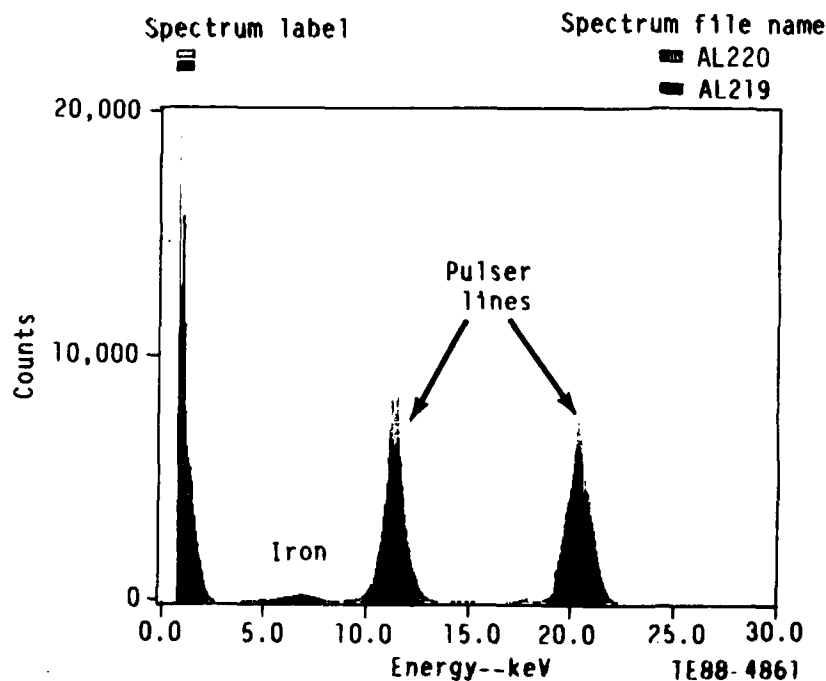


Figure 43. Spectra at 701 Hz lateral resonance with and without detector HV bias.

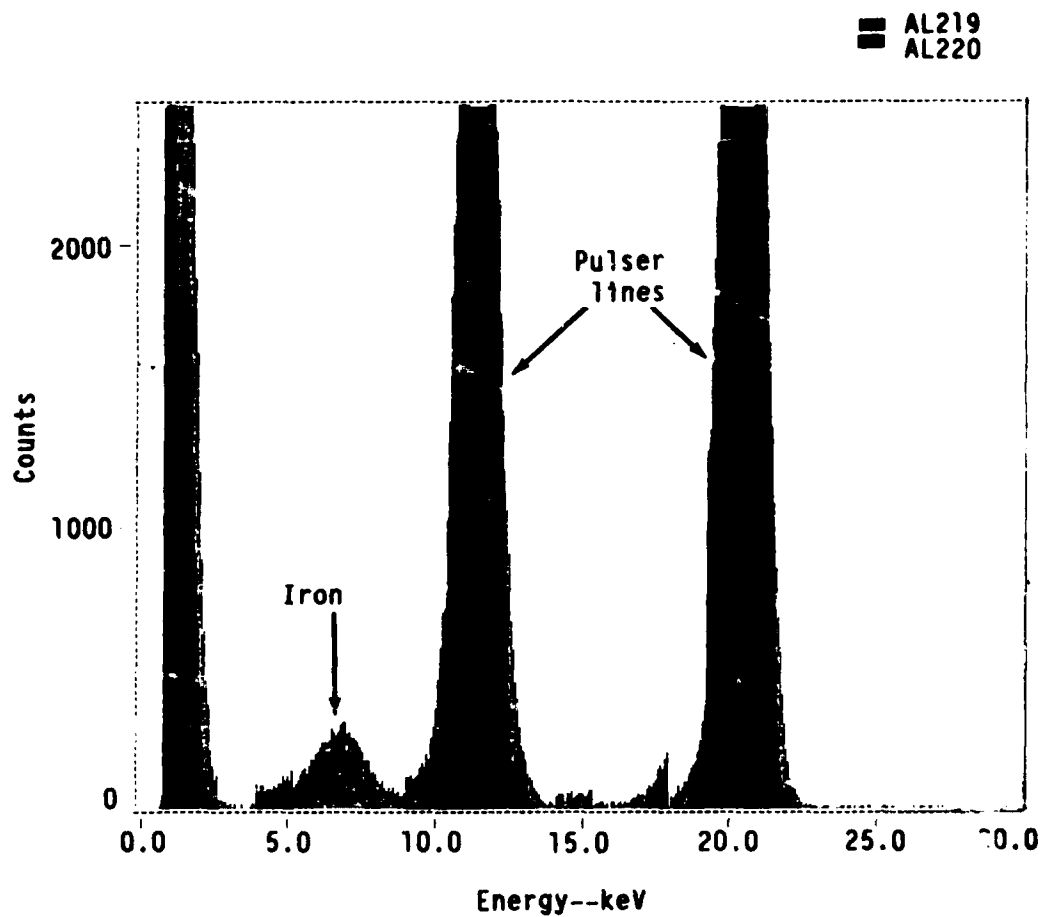
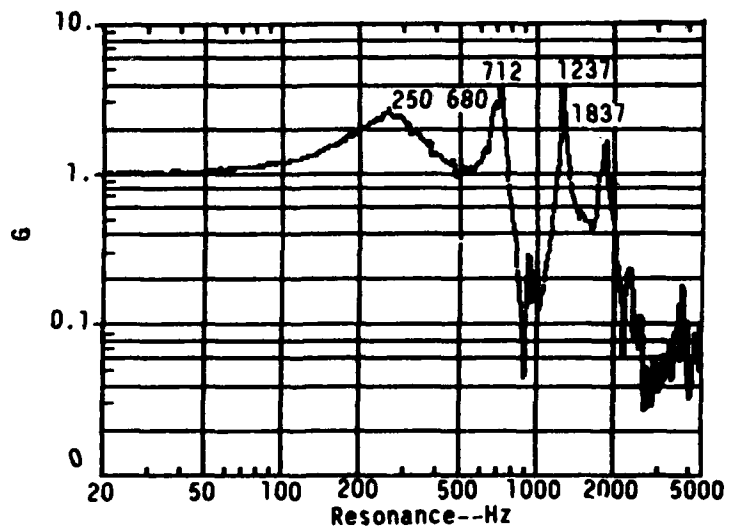


Figure 44. Expanded display of Figure 43. TE88-4862  
 TF41 oil wear monitor



Evaluation Unit 3, Test 5 Log x-axis  
 Last response channel 2 Sweep rate 400 lines  
 1.000 octave/minute  
 TE88-4863

Figure 45. Resonance profile--vertical vibration sweep, copper foil cell window replaced, circuit boards conformally coated.

Since this is now the original configuration, this profile should match the original Figure 31 data. Therefore the 712 Hz resonance should match the original 732 Hz resonance and similarly the 1237 Hz resonance match the original one at 1235 Hz.

Spectrum A1 223, Figure 46, and spectrum A1 224, Figure 45, were taken at 680 Hz and 712 Hz resonance peaks.

The sharp pulser resolution of Figure 40 is badly degraded and low energy background noise is entering the spectra.

The effects are particularly bad at 712 Hz (Figure 47).

However, the original equivalent resonance at 732 Hz had produced the horrendous spectrum shown in Figure 33, so if Figure 39 were compared with Figure 33, it would seem that conformal coating of components had a definite effect.

The computer display comparison of spectrum A1 208 Figure 33 and A1 224 Figure 47 is shown in Figure 48.

As in the original test, the sensor handled the stronger resonance at 1237 Hz much better as can be seen in spectrum A1 225, Figure 49, which might be compared with the original Figure 34.

The computer displayed comparison of spectrum A1 209 Figure 34 and A1 225 Figure 49 is shown in Figure 50.

Although conformal silicone coating of the electronics has definitely helped, a still more fundamental problem was to be found.

### 6.2.3 Test III--NAVMAT P-9492 Workmanship Profile Test

This is a standard random frequency test used to establish component and circuit board integrity under 10 minute tests in 3 axes.

The test profile is shown in Figure 51. Power levels are computer controlled to keep the profile between the displayed limits.

The sensor resonance responses were observed in the three mounting positions of vertical, lateral, and axial as described earlier.

Resonance profiles for the vertical, lateral, and axial vibrations tests are shown in Figures 52, 53, and 54 respectively.

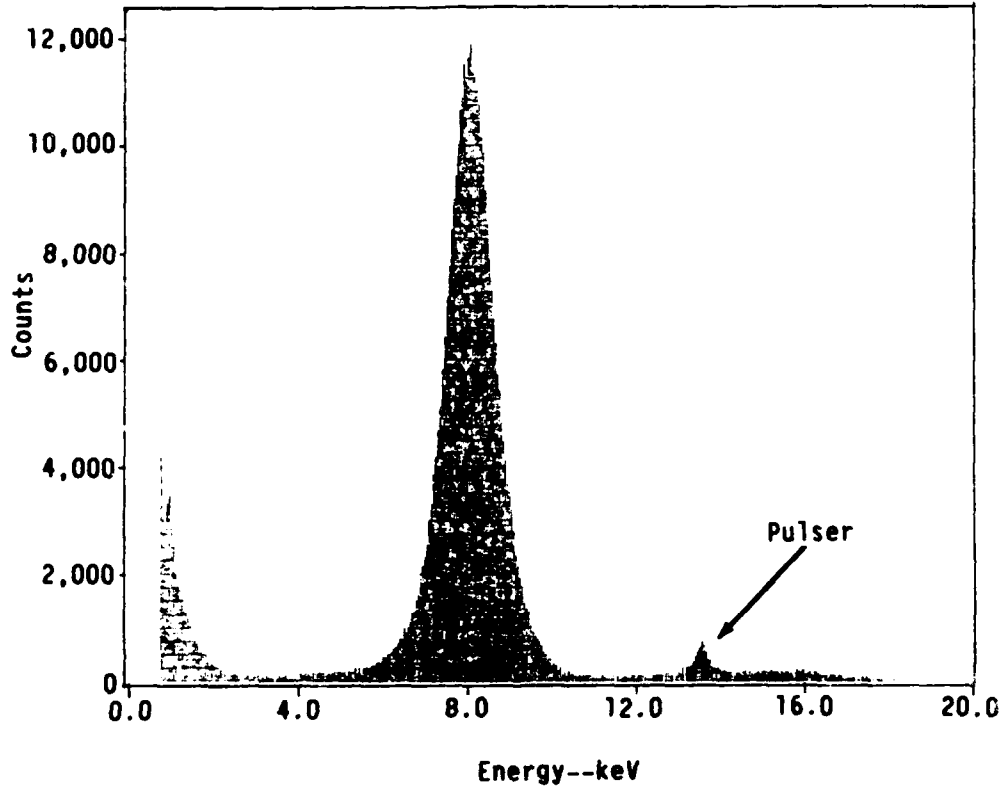
The response profiles are quite different for the three axes.

In all cases the sensor showed considerable background noise pickup of the form described earlier, although the sensor functioned normally throughout these tests.

Under these conditions of random driven vibration, an examination of the sensor output baseline from the main channel amplifier showed a resonance frequency of around 20 kHz, which could be locked onto with the oscilloscope triggering. Since this frequency is in the pass band of the sensor amplifier, this was thought to perhaps be the major cause of the background noise problems.

Spectrum label  
627

Spectrum file name  
AL223



TE88-4864

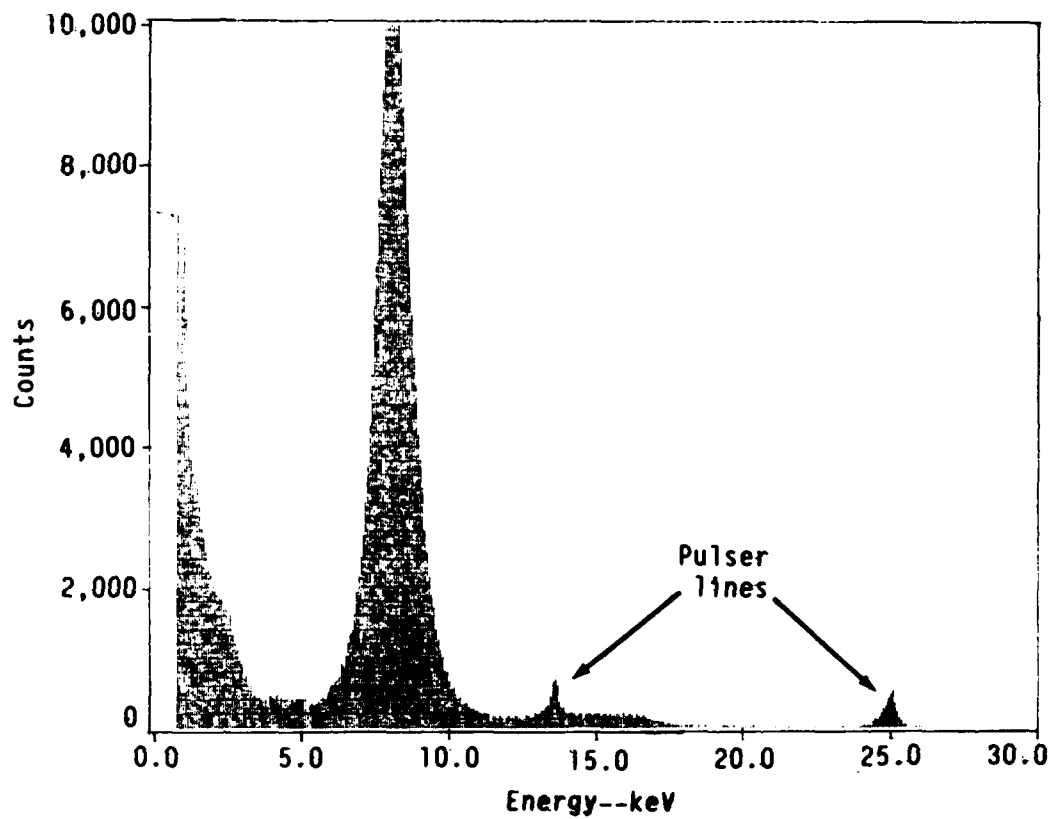
Figure 46. Spectrum at the 680 Hz resonance.

Spectrum label



Spectrum file name

AL224



TE88-4865

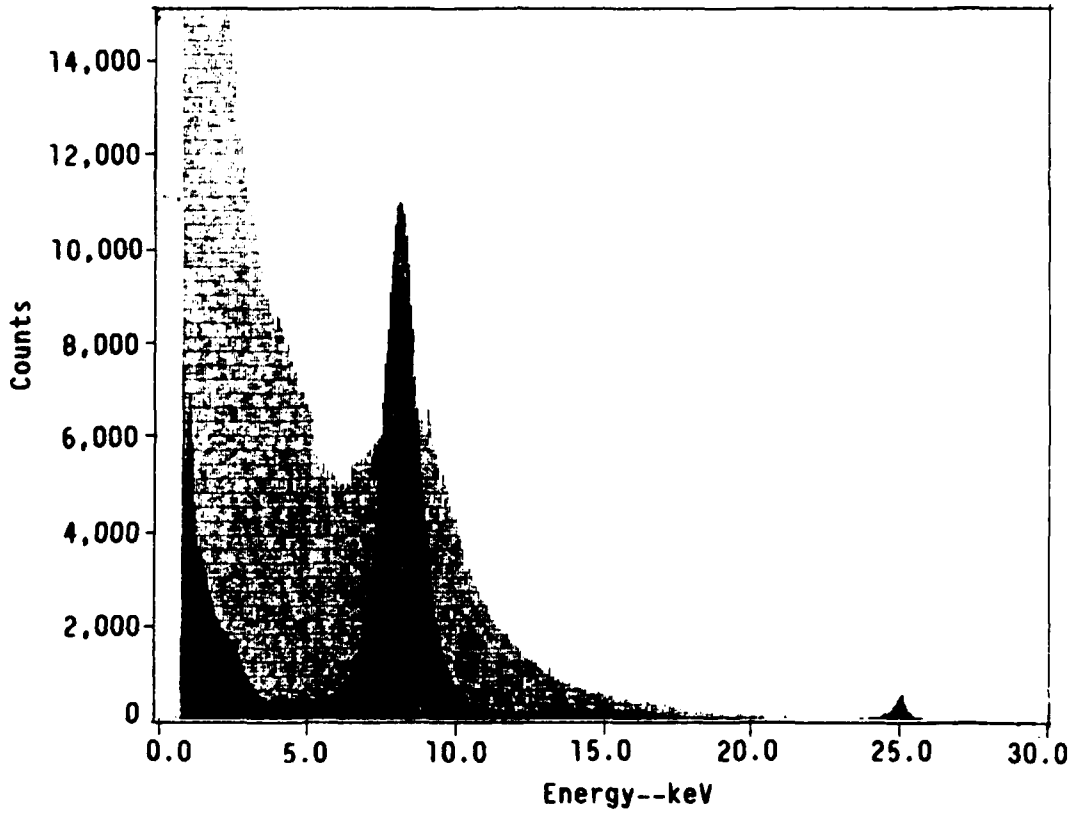
Figure 47. Spectrum at the 712 Hz resonance.

Spectrum label

AL208  
AL224

Spectrum file name

AL208  
AL224



TE88-4866

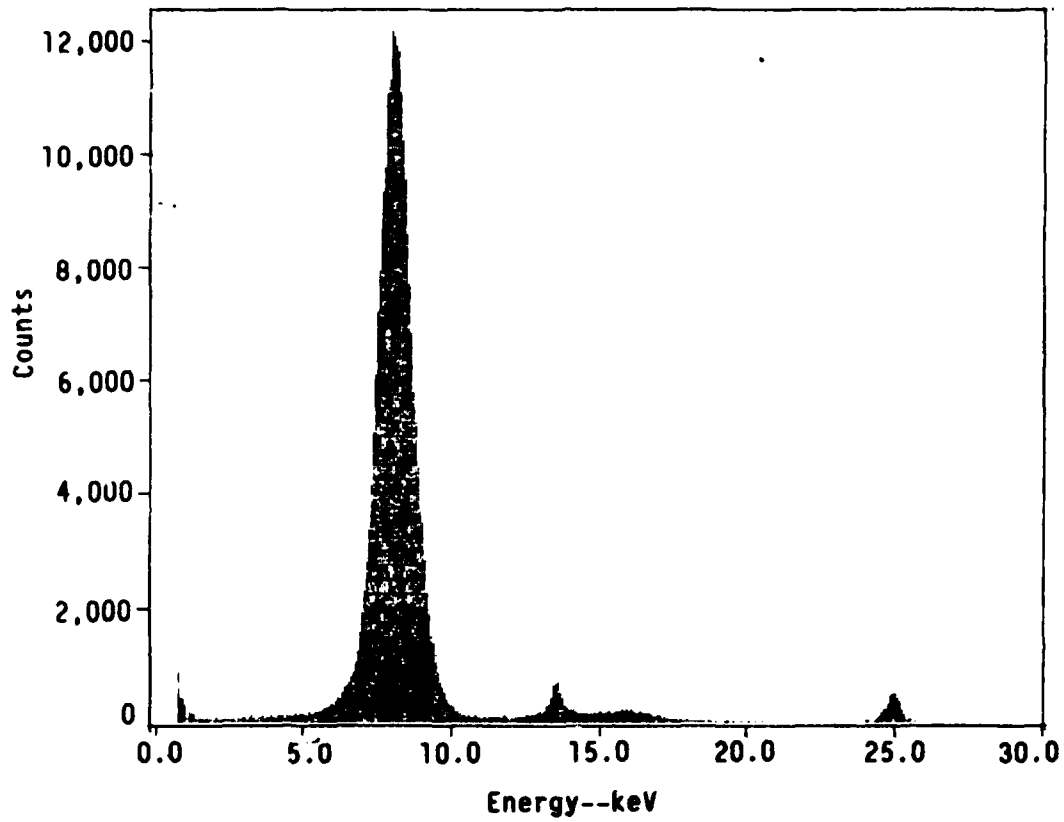
Figure 48. Comparison of Al 208 (Figure 33) and Al 224 (Figure 47).

Spectrum label

☐

Spectrum file name

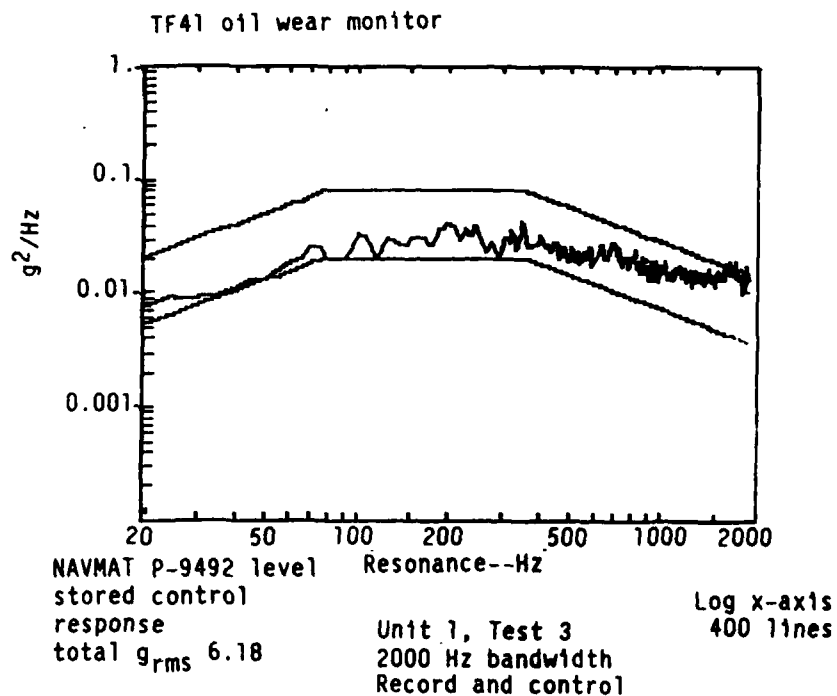
AL225



TE88-4867

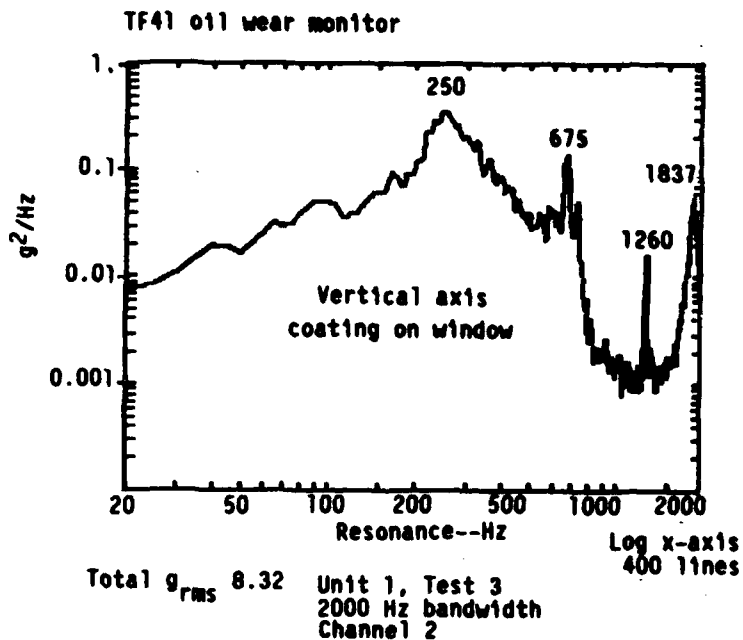
Figure 49. Spectrum at the 1237 Hz (5.9 g) resonance.





TE88-4869

Figure 51. NAVMAT vibration profile.



TE88-4870

Figure 52. Resonance profile--vertical vibration NAVMAT.

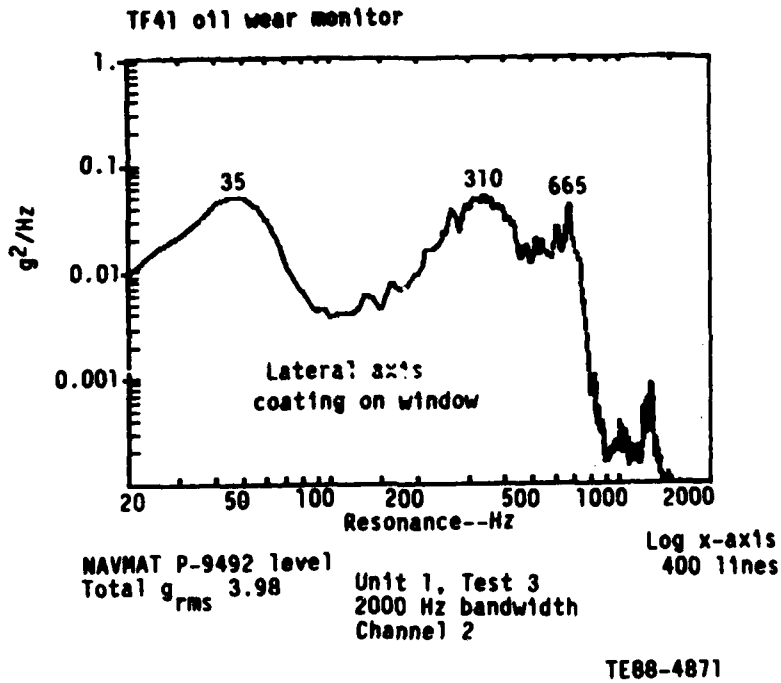


Figure 53. Resonance profile--lateral vibration--NAVMAT.

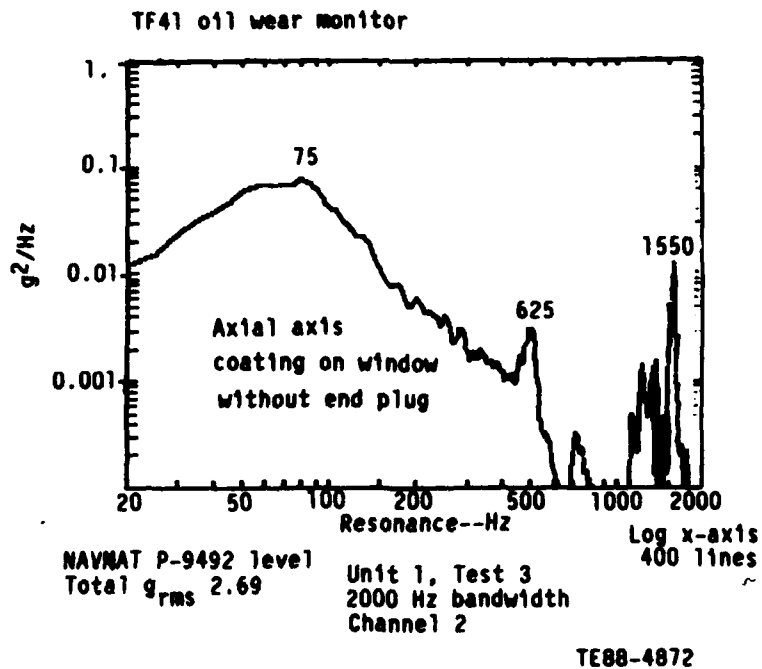


Figure 54. Resonance profile--axial vibration--NAVMAT repeated test.

A spectrum from the sensor working under these NAVMAT test conditions is shown in Figure 55.

In these tests the copper X-ray line has a high intensity and dominates the background.

Although some of the spectra in the report look quite good in terms of the analysis of the copper line, the actual required analysis of low ppm Fe levels (at 6.4 keV) would be at background intensity levels and would clearly have been hopelessly impossible in most cases--such as Figure 55 for example.

It appears that the final instrument will probably need some background curve fitting routines in the data analysis, even after the background noise problem is significantly improved; and unless it can be very significantly improved the sensor would not be able to detect ppm levels under these conditions.

#### 6.2.4 Test IV--Sine Wave Response

To see what input power levels were needed to generate the 20 kHz component, single frequency vibrations were again used.

The 20 kHz response was obtained at 1 g at 600 Hz and 1575 Hz. These frequencies correspond to the resonances either side of 1 kHz.

At 200 Hz the 20 kHz component was detected at 6 g's, and at 100 Hz and 28 Hz input levels of over 5 g's were needed.

This indicated that the sensor electronics could be affected at arbitrary frequencies if driven hard enough, and that the 20 kHz frequency generation was a constant effect.

#### 6.2.5 Test V--Sensor Box Response

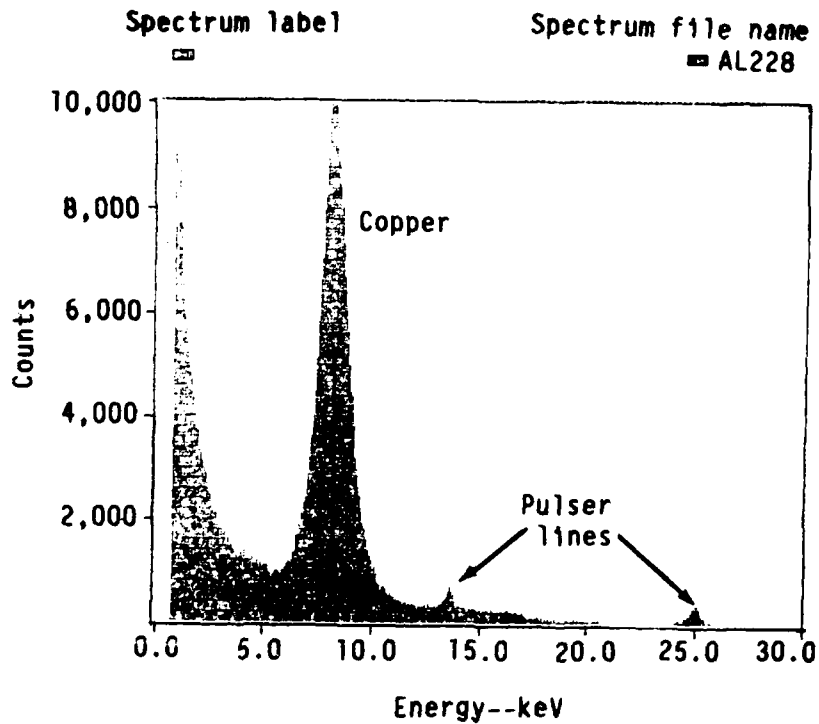
In this test the electronics sensor box was removed from the stainless steel cell body and clamped directly to the shake table baseplate.

The purpose of this test was to see which resonances were related to the sensor head compared with the fairly heavy cell and end couplings. The standard sine wave sweep was run and the sensor response curve is shown in Figure 56. There are no low frequency resonances and, as expected, system resonance frequencies were higher, and some of them (2775 Hz) were over 38 g peak amplitude.

The sensor was operational during these tests and at the 1425 Hz 5 g resonance only small ripples were introduced in the baseline noise output from the sensor.

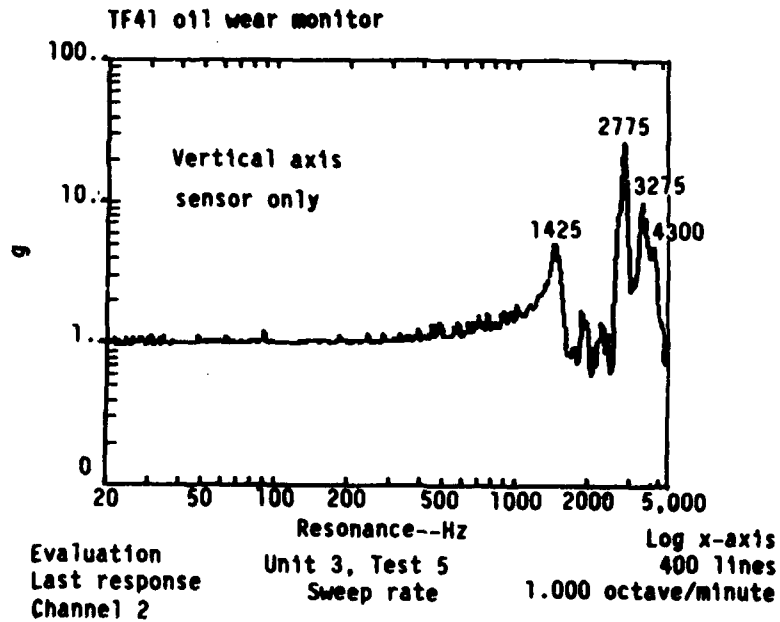
At the 2775 Hz resonance, however, there was a large several volt amplitude baseline frequency with a superimposed 20 kHz component of 0.8 V peak-to-peak amplitude.

This 2775 Hz resonance was thought to be due to the vibration of the top lid of the electronics compartment since some of the mounting screws were shaken out.



TE88-4873

Figure 55. Spectrum taken during NAVMAT vibration.



TE88-4874

Figure 56. Resonance profile--vertical vibration sweep sensor unit only--cell removed.

Spectrum Al 248 was taken at the 2775 Hz (38 g) resonance, as is shown in Figure 57. It was surprising to see anything analyzed at all under these conditions. The peak in the spectrum corresponds to analysis of Fe in the shaker table baseplate to which the sensor was clamped. The pulser lines are reduced to multiple bumps around 14 keV and 25 keV in the spectrum.

The HV bias to the detector was lowered and the 2775 Hz component decreased maybe 50 percent. It was concluded the 2775 Hz electronic signal resonance was most probably related to vibration of the HV distribution and filter board components. The ceramic filter capacitors are made from high K material and this also has piezoelectric properties.

Some method of handling this by selective mounting of these components must be worked out.

This still left the 20 kHz component, which was analyzed in the next test.

#### 6.2.6 Test VI--Engine Simulation Vibration Profile

The vibration profile shown in Figure 58 is considered to be a general TF41 engine test profile, basically a random distribution with two dominant engine frequencies superimposed. The computer system controlled the vibration profile within the boundary limits.

Under these conditions the sensor (still mounted directly to the shaker table baseplate) produced the 20 kHz component in the signal baseline output, with up to 1.5 V peak to peak amplitude. The response was in the form of a pulse envelope as sketched in Figure 59 and which can be interpreted as a series of 20 kHz signals induced at different amplitudes at different system frequency points (resonances) when accessed randomly.

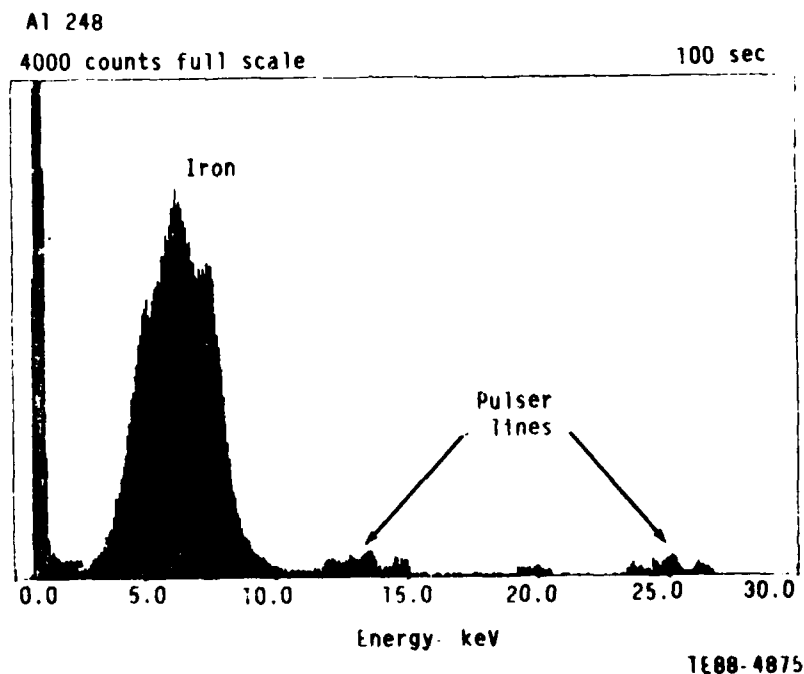
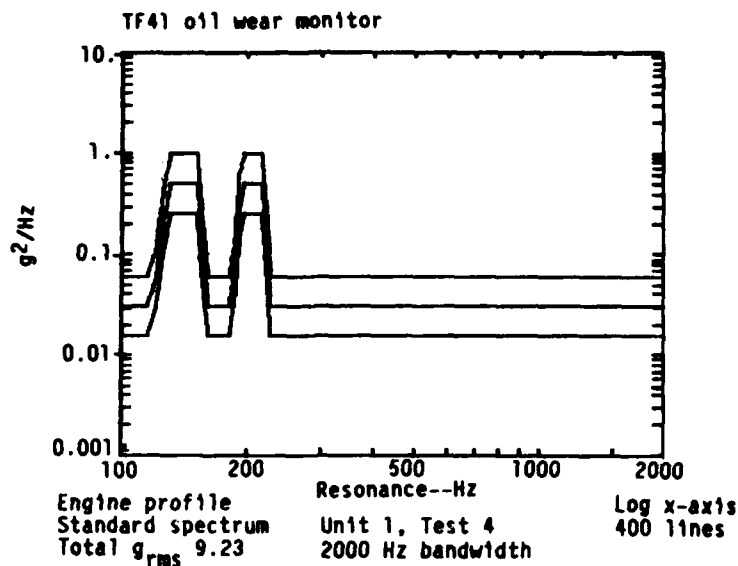


Figure 57. Spectrum at 2775 Hz (38 g) resonance.



TE88-4876

Figure 58. Simulated TF41 engine vibration profile.

This explains why the vibration effects in the sensor appear as a background noise sweeping into the spectrum to different levels, since the analyzer considers these as spectrum pulses. Randomly driven vibration seems the best way to observe the effect.

The first step was to remove the sensor from the shaker table, open the electronics compartment, and cut out the HV counter wiring and ground the counter tube.

The 20 kHz effect was still there unabated when the vibration test was re-established. The next step was to disconnect the counter completely from the input to the preamplifier section, and re-establish the vibration profile. The 20 kHz component was still clearly present although reduced to 0.6 V peak to peak maximum levels. Since the detector capacitance (estimated 3 to 4 pf) is now removed from the FET gate junction, we expected that the vibration induced effect would decrease.

Removal of the counter should also have removed possible detector related noise sources (due to vibration of counter wire support members for example).

It is unlikely that these effects would also be at exactly 20 kHz, and a distinct 20 kHz signal still remained when the counter was removed from the loop.

Consequently, although possible counter vibration effects cannot be ruled out, the feeling is that the prime suspect is gate structure vibrations in the FET input component of the preamplifier, possibly including the chip header itself since the gate lead connection was already made very short and sturdy in the design.

This concluded the vibration tests at Allison.

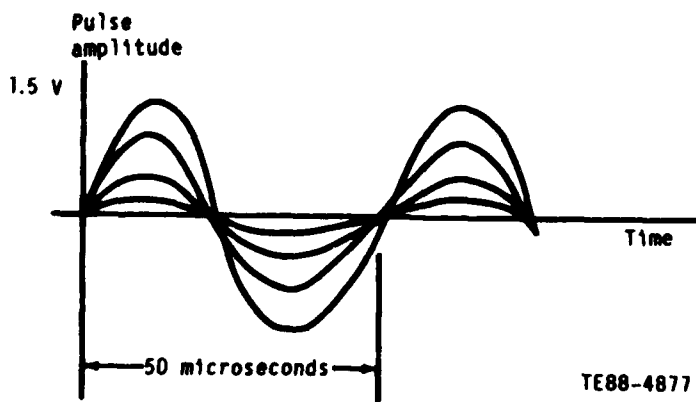


Figure 59. Pulse envelope.

## VII. SENSOR FLOW EVALUATION

In some engine oil analysis programs using flow cells the cell designs had been quite sophisticated to establish a flat oil flow pattern below the cell window, without restricting oil flow rates in the system.

There was concern that there might be problems with the fairly simplistic PGT design, which uses an anvil-shaped platform to, basically, scoop a section of the oil flow and roll it back over the window in a 6-mm thick layer.

A second cell had been fabricated with a viewing window, and this was installed in an oil flow pumping system constructed at Allison as part of this program for evaluating the sensor at various flows, temperatures, and contaminant concentrations.

It appears that oil flow across the window is wide and flat over a wide range of pumping speeds, and the design should be satisfactory.

At flow rates of 10 gallons per minute and above there were oil bubbles in the oil stream. This was due to air intake because the oil return line to the storage tank was above liquid level. However in an engine, where oil is pressure fed to the bearings and sprayed around the housing, there would be significant aeration.

There is obviously going to be some effect on analysis due to the presence of air. With an "infinite thickness" sample this may not be a serious problem with the XRF technique.

Since the oil flow system still had a few minor areas to be worked on and was in an inconvenient location in another building, and also because calibrated oil standards needed to be prepared, it was felt a temperature and flow system run with an installed working sensor should not be performed at Allison immediately after the vibration test.

It was agreed that the pumping system would be shipped to PGT along with the Conostan standard solutions and also MIL-L-23699 engine oil so that PGT could set up the system and prepare the standard samples for "spiking" of the oil flow during analysis.

In these tests it is planned to introduce aeration in some way to see what the effect is on analysis.

## VIII. CONCLUSIONS AND PLANS

The program has so far accomplished the following:

- o A preamplifier circuit for conditioning and amplifying the signals from a proportional counter X-ray detector tube has been developed and shown to be stable at the high ambient temperatures present on a turbine engine.
- o A high voltage power supply circuit for use with a proportional counter tube has been developed and shown to be stable at high ambient temperatures.
- o A sensor consisting of a flow cell that can be mounted on a TF41 engine, a miniature proportional counter tube, and miniature preamplifier and amplifier circuitry has been developed. The sensor has been demonstrated to have low enough background and high enough sensitivity to be capable of detecting iron down to the 2-5 ppm level with static oil samples.
- o The sensor has been vibration tested and was not damaged by sinusoidal or random vibration typical of a TF41 engine environment. Vibration resonance problems have been identified and are being worked.
- o The sensor flow cell with a clear plastic window in place of the X-ray permeable window has been evaluated on a flow rig and was found to create an even flow across the window over a wide range of flow rates.

The following activities are planned for the remainder of the program:

- o The sensor preamplifier input circuit is being redesigned to try to reduce vibration effects and will be retested to determine if the 20 kHz baseline noise has been attenuated.
- o The sensor will be flow tested at various flow rates, oil temperatures, and with various concentration levels to determine stability and correspondence with actual metal concentration values.
- o The sensor will be tested on an upcoming TF41 endurance test to determine the actual vibration profile on the engine and to check correspondence with engine oil metal concentration values.

#### REFERENCES

1. Packer, L. L., and Miner, J. R., AFAPL-TR-75-6, "X-Ray Wear Monitor," AFAPL Contract No. F33615-74-C-2024, January 1975.
2. Packer, L. L., AFWAL-TR-83-2029, "X-Ray Wear Metal Monitor," AFWAL Contract No. F33615-81-C-2065, December 1981.